Anisotropy and heterogeneity of microstructure and mechanical properties in metal additive manufacturing: a critical review

Y. Kok[a], X.P. Tan[a,*], P. Wang[c,*], M.L.S. Nai[c], N.H. Loh[b], E. Liu[a,b], S.B. Tor[a,b]

[a] Singapore Centre for 3D Printing, School of Mechanical and Aerospace Engineering, Nanyang Technological University, 50 Nanyang Avenue, 639798, Singapore

[b] School of Mechanical and Aerospace Engineering, Nanyang Technological University, 50 Nanyang Avenue, 639798, Singapore

[c] Singapore Institute of Manufacturing Technology, 73 Nanyang Drive, 637662, Singapore

* Corresponding authors. E-mail: xptan1985@gmail.com & xptan@ntu.edu.sg (X.P. Tan)

wangp@simtech.a-star.edu.sg & wangpangh@gmail.com (P. Wang)

Abstract

Metal additive manufacturing (AM) has developed rapidly over the last decade to become a disruptive technology capable of revolutionizing the way that products from various industrial sectors such as biomedical, aerospace, automotive, marine and offshore are designed. Early adopters of the technology like the biomedical and aerospace industries have shown that the better-designed components offer substantial performance improvements over current designs. However, in-depth and comprehensive views on the microstructure and mechanical properties of additively manufactured metals and alloys are less reported. To realize the full design potential that metal AM can offer, especially for load-bearing structural components, it is imperative to provide a thorough understanding on the anisotropic and heterogeneous microstructure and mechanical properties that often occur within metal AM parts. This paper outlines a broad range of metal AM technologies and reviews literatures on the anisotropy and heterogeneity of microstructure and mechanical properties for metal AM parts. It can be highlighted that the contributing factors to the anisotropy and heterogeneity within metal AM parts were either their unique microstructural features or manufacturing deficiencies. Concluding remarks on the state-of-the-art research regarding this topic and the possible solutions to overcome the anisotropy and heterogeneity of metal AM parts are provided.

1. Introduction

Metal additive manufacturing (AM), popularly known as metal three-dimensional (3D) printing, is a process of joining metallic materials (in powder, wire, sheet forms, etc.) to make

objects from 3D models usually layer upon layer [1, 2]. Metal AM has the potential of revolutionizing how metallic items are designed and constructed in the digital industrial era [3-5]. Sales of metal AM systems have been increased dramatically over the past few years [6]. Moreover, technologies have become increasingly mature for industrial adoption [7]. Correspondingly, there is an obvious boom in research interest in the area of metal AM, particularly in the last five years [8].

Most of studies have clearly stated benefits of metal AM technology, while there are still some limitations such as anisotropy and heterogeneity in microstructure and mechanical properties [9]. Anisotropy depicts a variety of orientation-dependent features of a material, while heterogeneity is defined as uniformity in its features. Recent studies have found that metal AM parts exhibited anisotropy and heterogeneity in microstructure and mechanical properties [10-15]. In conventional practice, superior and consistent mechanical properties of metal AM parts are prerequisites for engineering applications [16-18]. The use of functionally graded materials (FGM) is less common in conventional applications, though recent research has suggested that FGM are a possible way to meet future demands of the modern industry [19]. There have been extensive studies on the microstructure, mechanical properties, and processability of various metals and alloys in a variety of metal AM systems [8, 9, 20-22]. In particular, the formation of anisotropic and heterogeneous microstructure and its influence on mechanical properties are becoming hot research topics in metal AM field [9, 23-25].

Metal AM parts usually undergo complex cyclic thermal history consisting of directional heat extraction, repeated melting and rapid solidification [21, 26], which would create anisotropic and heterogeneous microstructures that intrinsically differed from the metallic parts manufactured via conventional methods [11, 12]. As a result, anisotropic and heterogeneous properties may occur in metal AM parts. In addition, AM defects such as pores, rough surfaces and lack of fusion layers, etc., would also induce the anisotropic and heterogeneous properties of metal AM parts [27, 28]. This paper will review the published literatures regarding the anisotropy and heterogeneity in microstructure and mechanical properties of metallic parts manufactured by the various metal AM techniques. The main objective is to better understand the microstructure and property of as-built AM materials so that direct manufacturing of metallic parts could be achieved in the short run.

2. Metal AM systems

2.1 Classification

The American Society for Testing and Materials (ASTM) international committee F42 on AM technologies classified AM technologies into 7 process categories in total [29]. The categories pertaining to metal AM are the following directed energy deposition (DED), powder-bed fusion (PBF), and sheet lamination (SL). The abbreviations of metal AM systems mentioned in this paper are listed in Table 1. Figure 1 shows a summary of the metal AM methods for each category.

Table 1. Abbreviations of metal AM terms mentioned in this paper (in alphabetic order).

Nomenclature	
DED	Direct energy deposition
DMLS	Direct metal laser sintering
EBF^3	Electron Beam Freeform Fabrication
EBM	Electron beam melting
LF3	Laser Free-Form Fabrication
LENS	Laser engineer net shaping
LMD	Laser metal deposition
LOM	Laminated object manufacturing
PBF	Powder bed fusion
SL	Sheet lamination
SLM	Selective laser melting
SLS	Selective laser sintering
SMD	Shaped metal deposition
UAM	Ultrasonic additive manufacturing

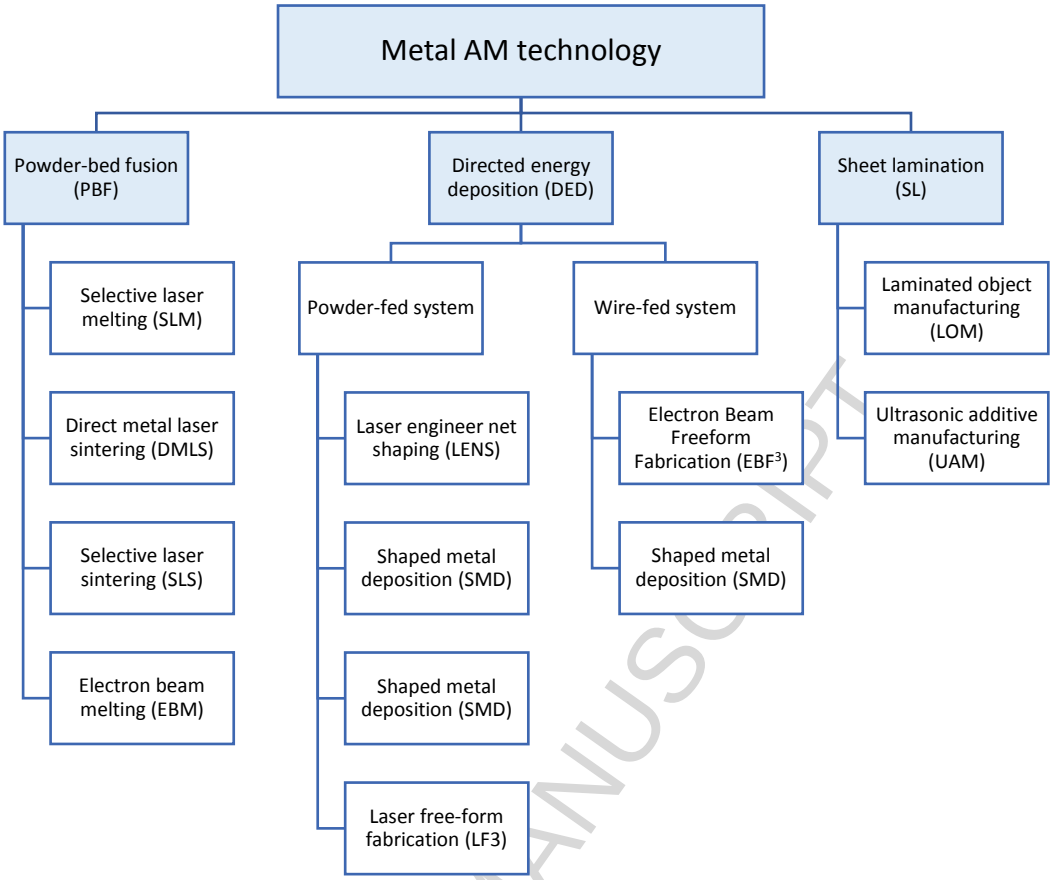

Figure 1. Summary of metal AM systems.

2.1.1 Powder-bed fusion (PBF)

PBF processes typically involve selective sintering or melting of powder materials using either a laser or an electron beam based on a powder-bed [30]. The laser beam imparts energy to the metallic powder via the absorption of radiation, while the electron beam works via the kinetic collisions between electrons and powder [31]. At the beginning of the process, a fresh layer of metallic powder was spread evenly using a rake or roller mechanism. The high-energy laser/electron beam then selectively melted the deposited layer of powder. After a layer was built, build table was lowered and the cycle repeated till the part was fully fabricated.

A generic schematic of a PBF system is shown in Figure 2. There are a number of laser-based AM techniques such as Laser Cusing, Direct Metal Laser Sintering, Selective Laser Sintering and Selective Laser Melting, though they are all essentially share a similar working principle [8]. The term “SLM” will be used to refer to all laser-based AM techniques under the PBF process for clarity in the following section. Unlike the SLM technologies, Arcam AB (Mölndal, Sweden) is currently the only commercial manufacturer of electron beam-based PBF systems, i.e. EBM.

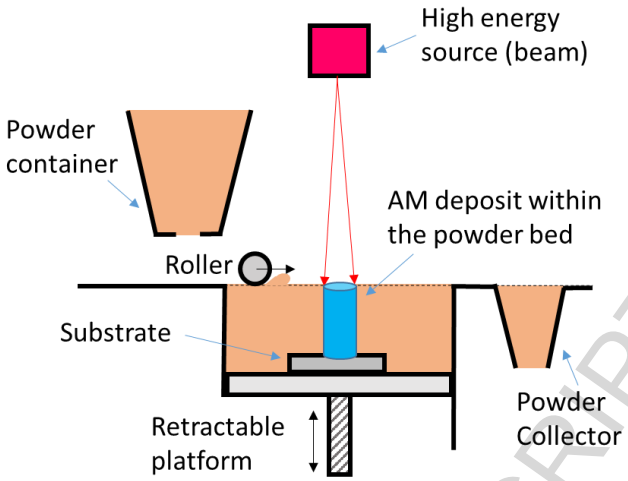

Figure 2. Generic illustration of a PBF AM system [32].

2.1.2 Directed Energy Deposition (DED)

DED processes cover the following systems such as Laser Engineer Net Shaping (LENS), Direct Metal Deposition (DMD), Laser Metal Deposition (LMD) and Shaped Metal Deposition (SMD). The DED process can be further sub categorized according to their material feedstock mode (i.e. powder-fed systems and wire-fed systems) as shown in Figure. 1.

Generic illustrations of the DED powder-fed system and wire-fed system are shown in Figure 3. DED process is a category of AM techniques that use a focused beam or an electric arc to fuse metallic powder or wire materials feedstock by layer-wise melting [20, 33]. Metal parts fabricated by DED processes exhibited high cooling rate solidified microstructures [2]. The layer of material being deposited can vary between 0.1 to a few millimetres in thickness [20]. Powder-fed AM systems have shown unique advantages in repair of worn or damaged metal components as they are not restricted to a powder bed [34].

Of particular interest is that DED processes are capable of producing functionally graded (heterogeneous) parts due to its flexibility to change materials' compositions at each layer, by simply adjusting feeding materials and process parameters [2, 35]. Additionally, wire-fed systems have the highest deposition rates due to the feedstock of wire materials.

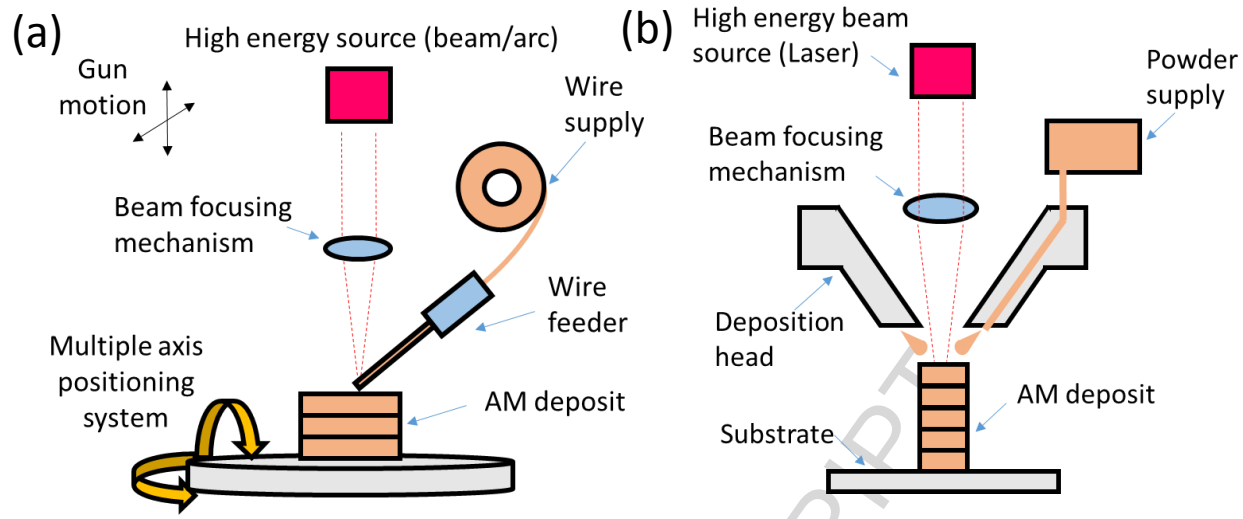

Figure 3. Generic illustrations of a DED AM systems: (a) powder-blown system, (b) wire-fed system [21].

2.1.3 Sheet Lamination (SL)

Sheet lamination processes include Ultrasonic additive manufacturing (UAM) and Laminated object manufacturing (LOM). Sheet lamination processes typically bond thin sheets of metallic foils by brazing, diffusion bonding, laser welding, resistance welding, or ultrasonic seam welding. A promising SL process is UAM, which uses ultrasonic vibrations to bond metal tapes into near net shape components [36]. Generic schematics of two SL AM systems are shown in Figure 4. An advantage of SL process is in its capability of processing different metal materials. The process does require additional post machining to remove unbound metals and to produce features such as channels and holes in order to achieve the desired geometry. Due to the joining of metal sheets, anisotropy in mechanical properties was prevalent in SL parts [20]. This is mainly due to the weaker bonding formed across the foil interfaces as compared with the intergranular bonding within each foil tape [2].

We found that each metal AM system may have their specific applications based on their own advantages. PBF systems are typically employed to produce complex geometries requiring high resolution and rigorous build accuracy. While DED systems are commonly applied to repair and refurbishment of metal parts and large-scale manufacturing. Lastly, sheet lamination systems have the capability of joining dissimilar metals to produce components with some specific properties.

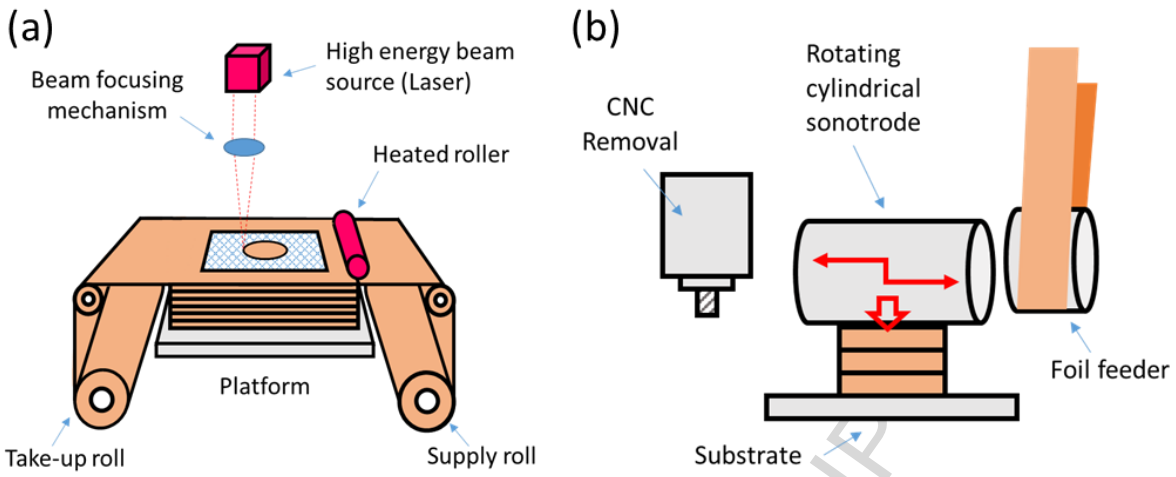

Figure 4. Generic illustrations of SL AM systems: (a) Laminated object manufacturing (LOM) [2] and (b) Ultrasonic additive manufacturing (UAM) [37].

2.2 Influence of processing variables on anisotropy and heterogeneity

A brief summary of the operating conditions and specifications of typical PBF, DED and SL systems is shown in Table 2. AM processing variables such as deposition rate, beam size, process temperature, deposition rates, deposition mode or scanning strategy, materials would result in differences in the microstructure of the as-fabricated part. The following sub sections will discuss such processing variables with regards to their influence towards anisotropy and heterogeneity of microstructures and properties for metal AM parts.

Table 2. Various operating conditions and specifications of PBF, DED and SL systems.

System	Build Volume (mm)	Energy Source	Preheat Temperature (^{0}C)	Beam Dia. (µm)	Deposition Rate/cc h^{-1}	Layer Thickness (µm)	Ref.
Powder-bed System							
Electron beam based							
Arcam (A2XX)	Ø420×300	3 kW Electron beam	up to 850 (Ti-6Al-4V, Co-Cr etc.)	~250	up to 60	50	[20, 38, 39]
Arcam (A2X)	200×200×380	3 kW Electron beam	up to 1100 (Ti-6Al-4V, Inconel, Ti-Al etc.)	~200	up to 80	25-90	[40-45]
Arcam (Q10)	200×200×180	3 kW Electron beam	up to 850 (Ti-6Al-4V)	~100	up to 80	50	[46]
Laser beam based							

SLM (SLM250)	250×250×250	400 W Nd: YAG laser	up to 200	~80	~20	10-50	[20, 47]
EOS (EOS 400)	400×400×400	1000W: fiber laser	up to 80	~80	~40	40	[28]
Concept Laser (M2)	250×250×300	200W: fiber laser	up to 80	70-200	~20	30	[48-50]
Powder-fed systems							
Optomec	900×1500×900	1-4 kW IPG fiber laser	-	~250	~230	250	[1, 20]
Wire-fed systems							
Sciaky (EBAM 300)	7620×2743×3353	>40 kW @ 60 kV welder	-	~380	~2000	3000	[1, 20]
Sheet lamination systems							
VHP UAM	1500x1500x600	9 kW @ 20 kHz	-	-	-	150	[51, 52]

2.2.1 Deposition rate

Some AM processes such as powder-fed DED are capable of producing material heterogeneity through in-situ variation in the deposition rate [53]. Figure 5a and b shows the result of a study that investigated the effect of deposition rates on the area fraction of equiaxed or columnar grains in the microstructure of DED titanium parts [53]. Though the reduction in deposition rate and beam size are often required to achieve better geometrical accuracy in such processes [2]. Figure 5c and d shows simulation results that supports the previous findings that the higher deposition rate results in the greater percentage of equiaxed grains. As a high deposition rate would correspond to a larger melt pool geometry and higher scanning velocity.

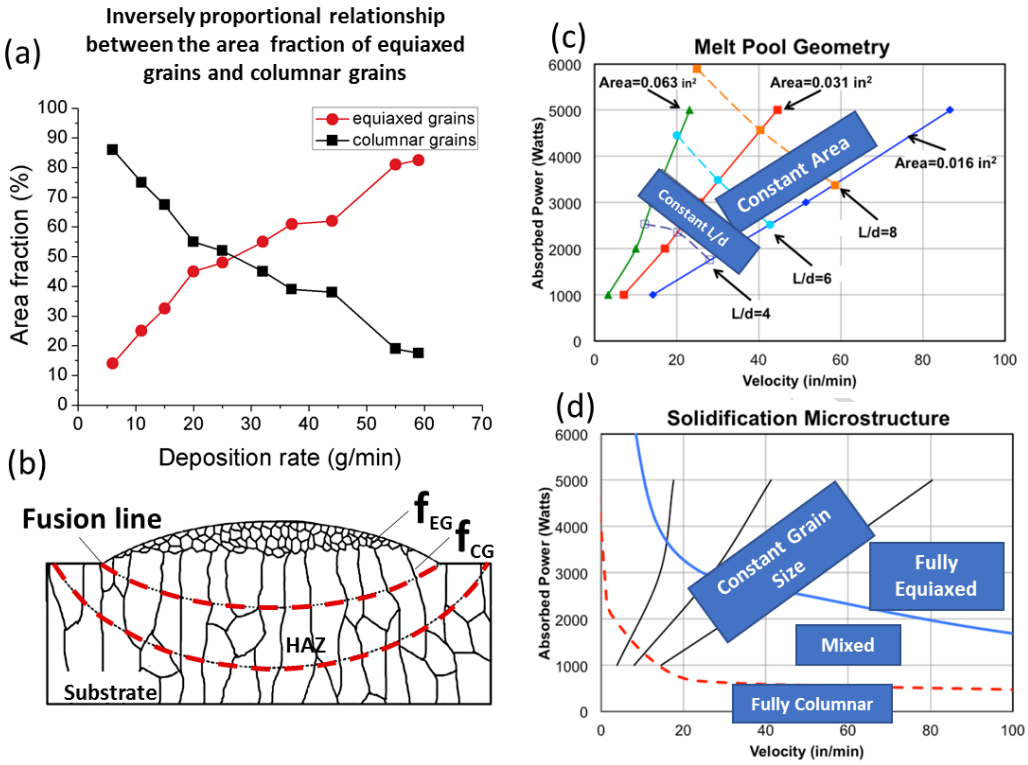

Figure 5. (a) A plot of the deposition rate against the area fraction of the equiaxed and columnar grains within a melt pool for the powder-fed DED process. (b) A schematic illustrating the measurements of area fractions of equiaxed and columnar grains f_{EG} and f_{CG} based on DED Ti–6.5Al–3.5Mo–1.5Zr–0.3Si alloy [53]. (c) Simulated Beam Power-Velocity process map for melt pool dimension control and (d) microstructure of a single bead deposit of electron beam wire-fed AM Ti-6Al-4V [54]. These show that the formation of a particular grain morphology can be controlled via the deposition rate.

2.2.2 Beam size and power

Beam size and power may influence particle ejection during the layer-wise melting process. There are three basic particle ejection modes in beam melting processes: (1) the convective transport of liquid or plasma metal out of the molten pool commonly called spatter ejection or sometimes referred to “fireworks” during the melting process, (2) kinetic recoil of powder in DED and (3) electrostatic repulsion of powder particles in EBM [20]. The former has been known to result in welding defects and is an underlying mechanism for the formation of process-induced porosity [20, 55]. Such defects can in turn affect the anisotropy and heterogeneity of the metal AM part.

2.2.3 Build environment

The AM build environment is an important processing variable. It was found that the absorption of atmospheric gasses during the building process might negatively impact the mechanical properties of the materials [56]. Thus, inert gas or vacuum atmosphere were often used during the metal AM processes [8]. However, operating in high vacuum environment will lead to an increased melt vaporization and outgassing of impurities [20, 57], which could cause heterogeneity in chemical composition. In addition, it was reported that the flow rate and the pathway of inert gas had an effect on the porosity in SLM-built Ti-6Al-4V [58] due to the fact that impurities generated from the melting process were re-deposited onto the scanned area.

2.2.4 Processing temperature

Processing temperature varies among the different metal AM systems. Some metal AM systems like LENS and UAM typically work at low process temperatures, while others such as EBM could require a processing temperature as high as ~1000 ^{o}C for some high-temperature materials [59]. Low substrate temperature in metal AM systems can reduce the heterogeneity in microstructure due to differences in part size [60]. However, the low substrate temperature could induce a higher magnitude of residual stress distributed unevenly in metal AM parts [61], which has been reported to negatively affect the bulk mechanical behaviour [20].

2.2.5 Deposition mode and scan strategy

Deposition mode is the way in which material is delivered onto the melt surface in the metal AM system. The angle at which the material is fed in DED processes has been shown to be significant to minimize the defects during melting [62]. In the case of PBF processes, the beam scanning strategy is the important factor for controlling build defects [63]. The scan strategies that are commonly used in PBF systems include bi-directional, snaking and checker box [64-66]. Scan strategies have been reported to influence the crystal texture of the grains due to differences in the overall direction of the thermal gradient [67, 68]. Crystallographic texture mainly contributes to anisotropy in the material [69, 70]. Other than crystallographic texture, scan strategy has also been attributed to be able to control the formation of either equiaxed or columnar grains, by altering the scan strategy across layers [71, 72]. As such it can be seen that deposition mode and scan strategy could play an important role in controlling the anisotropy and heterogeneity in metal AM parts.

2.2.6 Materials

Most of metal AM technologies such as PBF, DED and SL, adopt raw material in the forms of powder, wire and sheet. The quality of powder (e.g. morphology and size distribution)

used in PBF systems can determine the uniformity of powder spreading across the build plate [73, 74]. Such physical properties can also affect the density of metal AM parts [75]. The difference in the powder's quality is due to the different powder production methods [20]. Some powder production methods such as gas atomization can induce gas porosity into the final AM part. Post heat treatment processes (e.g. hot isostatic pressing) was needed to eliminate such pores [57]. The technology for the production of wire feedstock for the DED process is more mature as compared to the production of powder feedstock [20]. However, there still exist some defects relating to wire-type feedstock. Defects such as cracks or scratches on the wire surfaces can directly lead to porosity in the final AM part [20].

3. Anisotropy in metal AM

Metal AM systems allow the fabrication of near-net-shaped parts with excellent tensile properties [9]. Some researchers reported anisotropic mechanical properties in metal AM parts, while other researchers reported on the contrary [11, 76-81]. The discrepancy in the studies may be due to the complex microstructure that exists in metal AM parts [82, 83]. This section thus aims to discuss the relationship between microstructure and mechanical properties on anisotropy.

3.1 Anisotropy in microstructure

3.1.1 Grain morphology

A common microstructure feature observed in metal AM parts was the epitaxial columnar grain morphology [11, 15, 38, 43, 84-86]. Figure 6 shows an example of the epitaxial columnar grain morphology in SLM Co-Cr-Mo-alloy via an SEM micrograph and its corresponding crystal orientation map [87]. Such columnar grains that are aligned parallel to the build direction have been mainly attributed to causing anisotropy of mechanical properties in metal AM parts [10]. In the build direction, the accumulation of slip dislocations along the prior β grain boundaries is greater as compared to the orientation perpendicular to the build direction due to the longer length of the prior β grain boundaries [88]. As such more plastic deformation before failure is generally reported in the vertically orientated samples [9]. Epitaxial columnar grain growth is because of the re-melting of previous layers during the material deposition process. It induced sufficient thermal gradient within the melt pool, which would prevent nucleation ahead of the solidification front [72]. It is worthwhile to note that the novel use of rolling deformation step to refine the columnar grains in AM-processed Ti-6Al-

4V alloy has been demonstrated to be effective in refining the grain size [89]. This could lead to new development to metal AM processes.

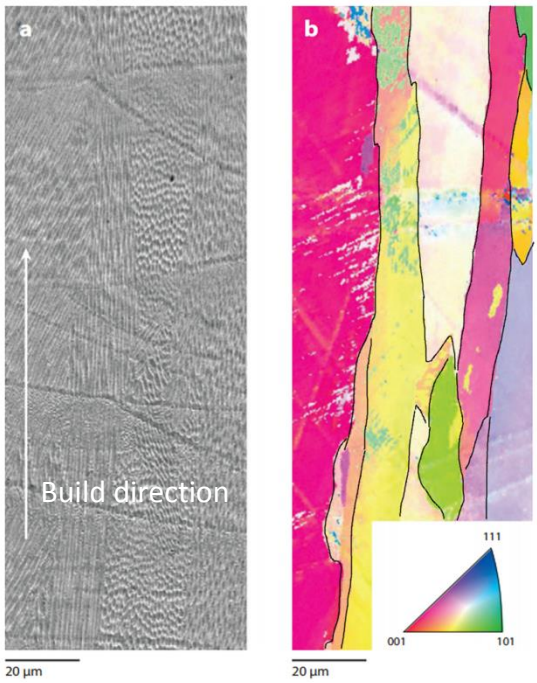

Figure 6. (a) SEM micrograph of the cross section of a Co-29Cr-6Mo alloy produced using the SLM process. (b) The corresponding crystal orientation map of the micrograph [87] showing the epitaxial columnar grain morphology in metal AM parts.

3.1.2 Crystallographic texture

Given the steep thermal gradient along the build direction, the EBM-built Ti-6Al-4V exhibited a preferential <001> crystallographic texture for the reconstructed prior β grains [90]. Figure 7 shows that the $<001>_{\beta}$ texture of the reconstructed prior β grains of EBM-built Ti-6Al-4V improved with build height due to the grains with a <001> orientation having the greatest growth advantage [90]. Strong crystallographic texture has been known to result in anisotropy in mechanical properties [91]. However, due to the phase transformation from β to α phase following the Burgers orientation relationship and a near random distribution of α phase across the 12 variants during the phase transformation, the resultant crystallographic orientation of the predominantly α phase showed an almost isotropic distribution [82, 85]. It is thus likely that the resultant crystallographic texture in the case of EBM-built Ti-6Al-4V may not be a significant contributor to anisotropy. Another study on laser based PBF tantalum likewise suggested that the elongated grain morphology along the build direction had a larger influence on the anisotropy as compared to the crystallographic texture [69].

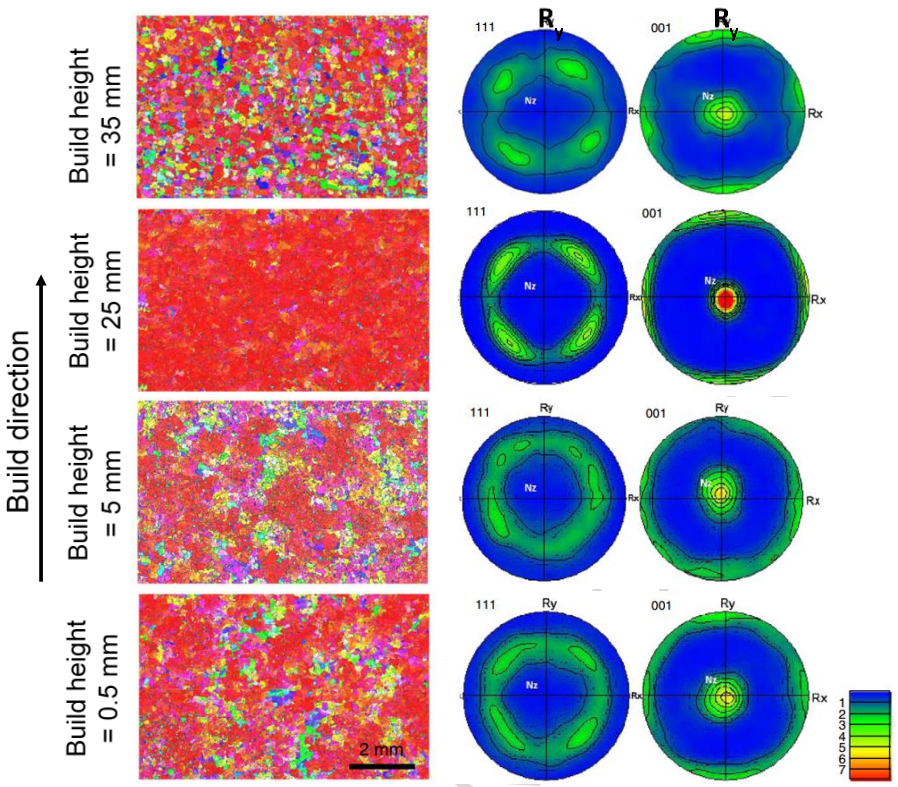

Figure 7. Reconstructed β-phase IPF maps and their corresponding texture pole figures for EBM-built Ti-6Al-4V alloy at different build heights of (a) 0.5 mm, (b) 5 mm, (c) 25 mm, (d) 35 mm near the build top surface [90] showing the heterogeneity in crystal orientation with build height.

3.1.3 Lack-of-fusion defects

Lack-of-fusion defects can be formed possibly due to unoptimized process parameters [92]. Such processing defects can range from ~50-500 µm in size [93]. More importantly, such defects often act as stress concentration sites as they are orientated perpendicularly to the build direction. The directionality of such defects plays an important role on the anisotropy in mechanical properties [27]. This is attributed to the tensile stress being normal to the plane of the defect, thus inducing crack propagation along the tip of the defect leading to material failure. As such, it is important to identify such processing induced defects during the AM process. Many are actively conducting research in the area of in-situ process monitoring, to identify such material discontinuities during the manufacturing process [93]. Post heat treatment process like HIP can eliminate a majority such lack-of-fusion defects from metal AM parts [9].

In summary, columnar grain morphology, crystallographic texture and lack-of-fusion defects are the three factors contributing to the anisotropy in the microstructure of metal AM part. With on-going research to improve the quality of metal AM parts, it can be foreseen that

such lack-of-fusion defects will be significantly reduced [9]. Therefore, the columnar grain and the strong crystallographic texture mainly contribute to anisotropy in metal AM parts.

3.2 Anisotropy in mechanical properties

The published literatures regarding the anisotropic mechanical properties (e.g. tensile, compressive, fracture and fatigue) from metal AM parts will be discussed in the following sections. The majority of the available results was based on AM-processed titanium alloys. Other metals or alloys (e.g. cobalt chrome (CoCr), Inconel superalloys, stainless steels and aluminium alloys, etc.) will also be discussed in this article. In addition, the article will examine whether the anisotropic mechanical properties of metal AM-processed parts could meet the minimum requirements for practical applications. As anisotropy is an orientation-dependent property, the orientation designation standard will be presented to provide clarity.

3.2.1 Orientation designation standard

In order to develop standards for AM, the ASTM international formed a committee in 2009 and the International Organization for Standardisation (ISO) formed a committee in 2013. Then the two organizations signed a partnership to jointly develop standards for AM [94]. This article will adopt the ISO and ASTM standard regarding the orientation designations for mechanical testing to provide consistency in comparison [94]. Figure 8a shows the orientation designation for mechanical testing based on the ISO and ASTM standard. In this terminology, rectangular test coupon requires three alphabets (X, Y, and Z) to provide a complete orientation designation. The X-axis is designated to be parallel to the front of the machine while the Z-axis is in the vertical direction. The Y-axis is perpendicular to both the X and Z-axis, with a positive direction following a right-hand rule coordinate system. The first alphabet in the designation corresponds to the axis parallel to the longest overall dimension and the second and third alphabets correspond to the axis parallel to the second and third longest overall dimensions.

Additionally, Figure 8b shows the possible ISO designations for determining the orientation dependence of mechanical properties for AM-processed samples based on a study [24]. The first letter in this nomenclature represents the directions normal to the crack plane, and the second letter represents the predicted direction of the crack propagation. The last letter represents the plane in which the crack begins (e.g. start (s), end (e), middle (m) and both (b)). These orientation designation standards thus provide a starting point for comparison of the published literature in the current work. Further standards to designate the orientation and

location dependent properties need to be developed given the reported heterogeneity in metal AM parts [9].

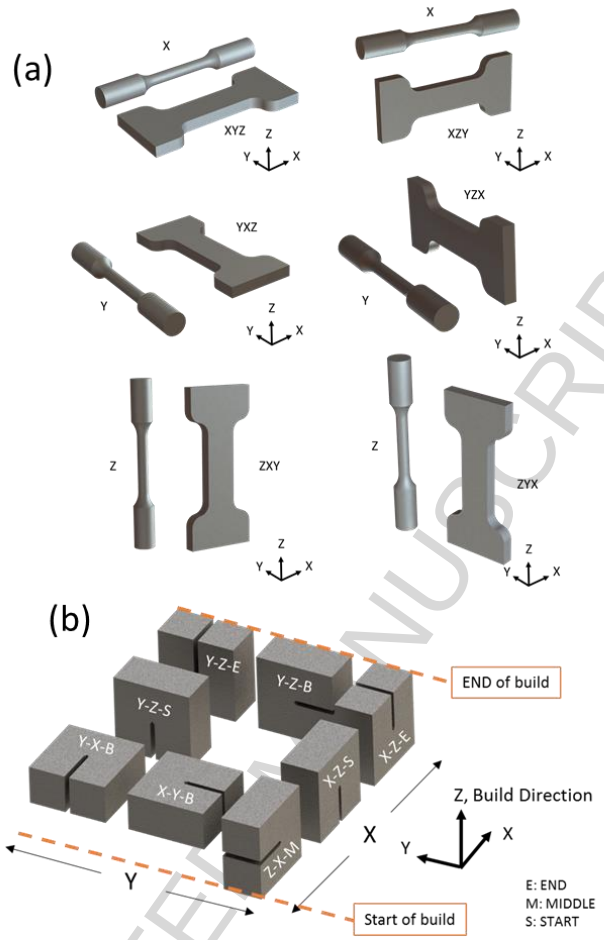

Figure 8. Orientation designations for mechanical testing of AM-processed materials, (a) tensile test [9] (b) determining the orientation dependence of mechanical properties [24].

3.2.2 Tensile properties

Many studies have shown that the tensile properties of AM-processed Ti-6Al-4V are comparable to their cast and wrought material equivalents [9, 11, 21, 95]. However, less emphasis has been placed on investigating the anisotropic mechanical properties of metal AM parts using various technologies. More importantly, it is still not well understood if the lower limit of anisotropic mechanical properties in metal AM parts could meet the minimum requirements of their cast and wrought equivalents. Table 3 summarises the anisotropic tensile properties of various metal AM parts. Anisotropy will be defined as $\frac{\sigma_x - \sigma_z}{\sigma_x} \times 100\%$ [96], where σ_x and σ_z denotes the mechanical properties (e.g. yield strength, elongation, fracture toughness and fatigue threshold) in the x and z directions, respectively. It is worth noting that the trend of

anisotropy is opposing for tensile strength and ductility [97]. In the majority of the studies on EBM-built and DED-built Ti-6Al-4V, no significant anisotropy in yield strength was observed [11]. However, in the case of SLM-built Ti-6Al-4V, there existed higher anisotropy in the yield strength between the different build orientations. Anisotropy in tensile properties was also observed in SL aluminium alloy [14]. Despite anisotropy being exhibited by the SLM-built Ti-6Al-4V, a majority of the reported yield strength either matched or surpassed the minimum values for their cast and wrought equivalents.

However, the majority of ductility results observed in SLM-built and DED-built Ti-6Al-4V was below the minimum value of 8-10 % elongation for wrought material. The low ductility of SLM-built and DED-built Ti-6Al-4V is mainly attributed to the brittle martensitic phase formed during the SLM and DED processes [10, 98]. By contrast, EBM-built Ti-6Al-4V parts usually have better ductility properties [11, 43, 84, 99]. It is noted that SLM, DED and EBM-fabricated parts all showed better ductility in the vertical orientation as compared to the horizontal orientation as can be observed by the high anisotropy percentages [11, 60]. Ductility of metal AM parts can be improved through post heat treatment processes [96, 100, 101]. In some studies, anisotropy in ductility remains between the different orientations, suggesting that the anisotropic property is most likely due to the columnar grains [11, 80, 97].

Table 3. Summary of tensile properties of various metal AM parts.

Material	Condition	Process	Tensile Axis Orientation	Anisotropy in yield strength (%)	Anisotropy in elongation (%)	Yield Strength (MPa)	Ultimate Tensile Strength (MPa)	Elongation (%)	Ref.
		Powder-bed fusion							
		Electron beam based							
Ti-6Al-4V	As-built	Arcam	Horizontal (XY)	-1.0	-14.0	870.0 ± 8.1	971.0 ± 3.1	12.1 ± 0.8	[102]
			Vertical (Z)			879.0 ± 12.0	953.0 ± 8.8	13.8 ± 0.9	
Ti-6Al-4V	As-built	Arcam A1	Horizontal (XY &YX)	-3.7	-33.3	783.0 ± 15.0	833.0 ± 22.0	2.7 ± 0.4	[81]
			Vertical (ZXY)			812.0 ± 12.0	851.0 ± 19.0	3.6 ± 0.9	
Ti-6Al-4V	Machined	Arcam S400	Horizontal(X/Y)	27.3	-98.0	1195.0 ± 19.0	1269.0 ± 9	5.0 ± 0.5	[103]
			Vertical (Z)			869.0 ± 7.2	928.0 ± 9.8	9.9 ± 1.7	
Ti-6Al-4V	As-built	Arcam S2	Horizontal (XY)	-0.1	26.2	982.9 ± 5.7	982.9 ± 5.7	12.2 ± 0.8	[79]
			Vertical (Z)			984.1 ± 8.5	1032.9 ± 12.9	9.0 ± 2.9	
Ti-6Al-4V	As-built	Arcam A2	Horizontal (XYZ)	23.6	-	825	907	-	[88]
			Vertical (ZXY)			630	792	-	
Ti-6Al-4V	HIP	Arcam	Horizontal (XYZ)	-0.2	5.1	866 ± 6.4	959 ± 8.2	13.6 ± 0.6	[102]
			Vertical (Z)			868 ± 2.9	942 ± 2.6	12.9 ± 0.8	

Ti-6Al-4V	As-built	Arcam A2X	Horizontal (XY)	-2.8	-28.6	~875	~950	~14	[11]
			Vertical (Z)			~900	~950	~18	
Ti-6Al-4V ELI	As-built	Arcam	Horizontal (XYZ)	0.0	-4.1	803	896	17	[104]
			Vertical (Z)			803	896	17.7	
Ti-6Al-4V ELI	As-built	Arcam	Horizontal (XYZ)	1.8	-9.5	817 ± 4.3	918 ± 1.0	12.6 ± 0.8	[102]
			Vertical (Z)			802 ± 7.9	904 ± 6.9	13.8 ± 0.9	
Ti-6Al-4V ELI	HIP	Arcam	Horizontal (XYZ)	0.9	-8.8	814 ± 2.4	916 ± 2.5	13.6 ± 1.2	[102]
			Vertical (Z)			807 ± 8.4	902 ± 8.7	14.8 ± 0.5	
CoCrMo	As-built	Arcam	Horizontal (XYZ)	-9.6	84.0	717	1110	5	[105]
			Vertical (Z)			786	869	0.8	
CoCrMo	HIP & HT	Arcam	Horizontal (XYZ)	0.2	0.0	586	1145	30	[105]
			Vertical (Z)			585	1151	30	
Laser beam based									
Ti-6Al-4V	As-built	SLM	Horizontal (XYZ)	-2.9	0.0	1093 ± 64	1279±13	6±0.7	[80]
			Vertical (ZXY)			1125 ± 22	1216±8	6±0.4	
Ti-6Al-4V	As-built	Renishaw AM250	Horizontal (XYZ)	10.0	-17.1	1075 ± 25	1199 ± 49	7.6±0.5	[97]
			Horizontal (XZY)	1.1	24.6	978 ± 5	1143 ± 6	11.8 ± 0.5	
			Vertical (ZXY)			967 ± 10	1117±3	8.9±0.4	
Ti-6Al-4V	Machined	EOS M270 SLM	Horizontal (X/Y)	4.4	2.2	1195 ± 19	1269±9	5±0.5	[103]
			Vertical (Z)			1143 ± 30	1219±20	4.89±0.6	
Ti-6Al-4V	Machined	SLM	Horizontal (XY)	15.4	77.6	1137 ± 20	1206±8	7.6±2	[101]
			Vertical (Z)			962 ± 7	1166±25	1.7±0.3	
Ti-6Al-4V	As-built	Concept Laser M2	Horizontal (XY)	1.9	-54.5	1070 ± 50	1250±50	5.5±1	[98]
			Vertical (Z)			1050 ± 40	1180±30	8.5±1.5	
Ti-6Al-4V	SR	SLM	Horizontal (XYZ)	1.1	-14.3	1145 ± 17	1187 ± 10	7 ± 2.7	[80]
			Vertical (ZXY)			1132 ± 13	1156 ± 13	8 ± 0.4	
Ti-6Al-4V	SR	Renishaw AM250	Horizontal (XYZ)	3.8	-37.1	974 ± 7	1065 ± 21	7.0 ± 0.5	[97]
			Horizontal (XZY)	2.2	22.6	958 ± 6	1057 ± 8	12.4 ± 0.7	
			Vertical (ZXY)			937 ± 9	1052 ± 11	9.6 ± 0.9	
Ti-6Al-4V	HT	SLM	Horizontal (XYZ)	0.9	-100.0	973 ± 8	996 ± 10	3 ± 0.4	[80]
			Vertical (ZXY)			964 ± 7	998 ± 14	6 ± 2	
Ti-6Al-4V	HT	SLM	Horizontal (XY)	2.0	11.8	944 ± 8	1036 ± 30	8.5 ± 1	[101]
			Vertical (Z)			925 ± 14	1040 ± 4	7.5 ± 2	

IN718	-	SLM	Horizontal (X/Y)	9.7	-7.9	816 ± 24	1085 ± 11	19.1 ± 0.7	[106]
			Vertical (Z)			737 ± 4	1010 ± 10	20.6 ± 2.1	
IN718	HT	SLM	Horizontal (X/Y)	2.9	-9.4	1222 ± 26	1417 ± 4	15.9 ± 1.0	[106]
			Vertical (Z)			1186 ± 23	1387 ± 12	17.4 ± 0.4	
Al-Si-10Mg	As built	SLM	Horizontal(XY)	0.1	-11.0	169 ± 1	272.8 ± 2.9	8.2 ± 0.3	[107]
			Vertical(Z)			168.8 ± 1.3	267	9.1 ± 0.5	
Al-12Si	As built	SLM	Horizontal(XY)	-1.7	50	270.1 ± 10	325 ± 20	4.4 ± 0.7	
			Vertical(Z)			274.8 ± 8	296.1 ± 20	2.2 ± 0.3	[108]
Al-12Si	HT	SLM	Horizontal(XY)	2.0	20.8	153.4 ± 5	228 ± 13	5.3 ± 0.7	
			Vertical(Z)			150.3 ± 17	210.1 ± 20	4.2 ± 0.3	[108]
Al-Si-10Mg	As-built	Concept Laser M2	Horizontal (X/Y)	4.0	16.7	250	330	1.2	[109]
			Vertical (Z)			240	320	1	
Al-Si-10Mg	-	Concept Laser M1	Horizontal(XY)	-	37.5	-	391 ± 6	5.55 ± 0.4	[110]
			Vertical(Z)			-	398 ± 8	3.47 ± 0.6	
CoCrMo	As-built	Dimetal-100	Horizontal(XY)	7.1	25.0	738 ± 9.9	1050 ± 12.2	5.2 ± 0.3	[111]
			Vertical(Z)			685.3 ± 10.5	970 ± 9.8	3.9 ±0.2	
			DED systems						
			Powder-fed deposition						
Ti-6Al-4V	Machined	Trumpf system	Horizontal (X/Y)	0.0	58.3	950 ± 2	1025 ± 10	12 ± 1	[112]
			Vertical (Z)			950 ± 2	1025 ± 2	5 ± 1	
Ti-6Al-4V	As-built	Tritons Laser Free-Form Fabrication (LF3)	Horizontal (XYZ)	41.5	73.4	892 ± 10	911 ± 10	6.4 ± 0.6	[96]
			Vertical (ZXY)			522	797 ± 27	1.7 ± 0.3	
Ti-6Al-4V	Machined	Tritons Laser Free-Form Fabrication (LF3)	Horizontal (XYZ)	2.6	29.6	984 ± 25	1069 ± 19	5.4 ± 1	[96]
			Vertical (ZXY)			958 ± 14	1026 ± 17	3.8 ± 0.9	
TC21(Ti6Al2Sn2Zr3Mo1.5Cr2Nb)	HT	LAM	Horizontal (X/Y)	2.6	-471.4	868	997	2.8	[113]
			Vertical (Z)			845	933	16	
Ti-6Al-4V	Machined	DED	Horizontal (YZX)	0.2	-28.4	960 ± 26	1063 ± 20	10.9 ± 1.4	[10]
			Vertical			958 ± 19	1064 ± 26	14 ± 1	
Ti-6Al-4V	ASTM F1472	As-cast				>758	>860	>8	[114]
Ti-6Al-4V	ASTM F1108	Wrought				>860	>930	>10	[115]

CoCrMo	ASTM F75	As-cast	450	655	8	[116]
CoCrMo	ASTM F1537	Wrought	517	897	20	[117]
Al-Si-10Mg		As-cast	160	325	3	[118]
IN718	AMS 5382	As-cast	758	802	5	[119]
IN718	AMS 5662	Wrought	1034	1241	10	[119]

* SR = stress-relieved, HT = heat-treated, HIP = hot isostatic pressing

3.2.3 Fracture toughness

Fracture toughness is a property describing the ability of a material containing a crack to resist fracture [120, 121]. Table 4 compiles the reported fracture toughness values of some metal AM parts from a variety of studies. In both SLM-built and EBM-built Ti-6Al-4V, anisotropy in fracture toughness was reported [23]. Anisotropy in fracture toughness had a strong influence on the propagation path of cracks [122]. In horizontally orientated samples, cracks propagated through the columnar grains while in vertically orientated samples, cracks propagated along the columnar grain boundary instead [23]. It is worth to note that the fracture toughness of EBM-built Ti-6Al-4V, was comparable to the ASM standard of 44-66 MPa $m^{1/2}$ and 88-110 MPa $m^{1/2}$ for wrought and cast Ti-6Al-4V, respectively [123, 124]. The lower toughness values observed in SLM-built Ti-6Al-4V is due to the fine acicular α′ martensitic microstructure that is brittle as compared to the α/β duplex microstructure observed in the EBM-built Ti-6Al-4V [125].

Additionally, residual stresses within the metal AM parts can lead to anisotropy in fracture toughness [80]. Such residual stresses can be reduced by post heat treatment processes such as HIP or stress relief treatment. A study based on SLM Ti-6Al-4V observed an increase in fracture toughness and the loss in anisotropy after HIP and stress relief heat treatments for SLM-built Ti-6Al-4V [80]. A study on EBM-built Ti-6Al-4V however reported a decrease in fracture toughness after heat treatment processes, which was due to the coarsening of the microstructure [23]. Thus, understanding of the as-built microstructures for the different metal AM systems is important in determining the post heat treatment schemes in order to achieve superior fracture toughness.

Table 4. Summary of fracture toughness of various metal AM parts.

Material	Condition	Process	Orientation	Anisotropy in fracture toughness (%)	Fracture toughness (MPa √m)	Ref.

		Powder-bed fusion				
		Electron beam based				
Ti-6Al-4V	As-built	Arcam A1	Horizontal (Y-X-B, X-Y-B)	7.3	110±7.4	[81]
			Vertical (Z-X-M, Z-Y-M)		102±8.9	
Ti-6Al-4V	As-built	Arcam A2	Horizontal (X-Z-E, X-Y-B, Y-X-B)	18.8	67-80	[24]
			Vertical (Z-X-M)		65	
		Laser Beam based				
Ti-6Al-4V	As-built	SLM	Horizontal (X-Y-B)	17.9	28±2	[80]
			Vertical (X-Z-E, Z-X-M)		16-23	
Ti-6Al-4V	As-built	MTT 250	Horizontal (Y-X-B)	3.1	66.9±2.6	[125]
			Vertical (Z-X-M, Z-Y-M)		41.8-64.8±16.9	
Ti-6Al-4V	SR	SLM	Horizontal (X-Y-B)	-10.7	28±2	[80]
			Vertical (X-Z-E, Z-X-M)		30-31±2	
Ti-6Al-4V	HT	SLM	Horizontal (X-Y-B)	-19.5	41±2	[80]
			Vertical (X-Z-E, Z-X-M)		49±2	
Al-12Si	As-built	SLM	Horizontal (X-Y-B)	18.8	46.7	[108]
			Vertical (X-Z-E, Z-X-M)		37.9	
Al-12Si	HT	SLM	Horizontal (X-Y-B)	11.1	21.7	[108]
			Vertical (X-Z-E, Z-X-M)		19.3	

3.2.4 Compressive properties

Compressive testing was also commonly used to evaluate the mechanical properties of metal AM parts [44, 126, 127]. A study on SLM-built tantalum alloy reported that compressive yield strength was higher in the vertical direction as compared to that in the horizontal direction. This is attributed to the varying crystallographic textures [69]. The mechanical properties of SLM tantalum alloy were found to be better than those fabricated by either electron beam furnace or powder metallurgy despite the anisotropic tensile strength [69]. Anisotropy in mechanical properties can be designed into a part through structural design [128]. A study on EBM builds (Ti-6Al-4V) showed that different lattice designs exhibited varying degrees of anisotropy [56]. Anisotropy in compressive strength was shown to be dependent on the unit size of the lattice structure [129].

3.2.5 Fatigue properties

The evaluation of fatigue properties is critical to understand how metal AM parts fail under cyclic loading. Table 5 provides a summary of the published data regarding fatigue properties of metal AM parts. It can be observed that higher fatigue strengths were exhibited in the horizontal orientation as compared to the vertical orientation in PBF systems. In general, SLM fabricated parts exhibited a higher Paris slope as compared to the counterparts EBM, indicating a higher fatigue crack growth rate [9]. The cycles to failure of the as-fabricated metal AM parts are significantly lower as compared to their wrought equivalent, due to the rough build surface and the presence of internal defects acting as crack initiation sites [9]. However, the fatigue strength of metal AM parts can be improved through post heat treatment and surface machining as shown in Figure 9 [9, 130]. In addition to surface roughness and internal defects, fatigue crack propagation was also found to be dependent on the crystallographic orientation of the grain containing the crack tip, the number of grain boundaries surrounding it and the direction of internal residual stress [97, 125].

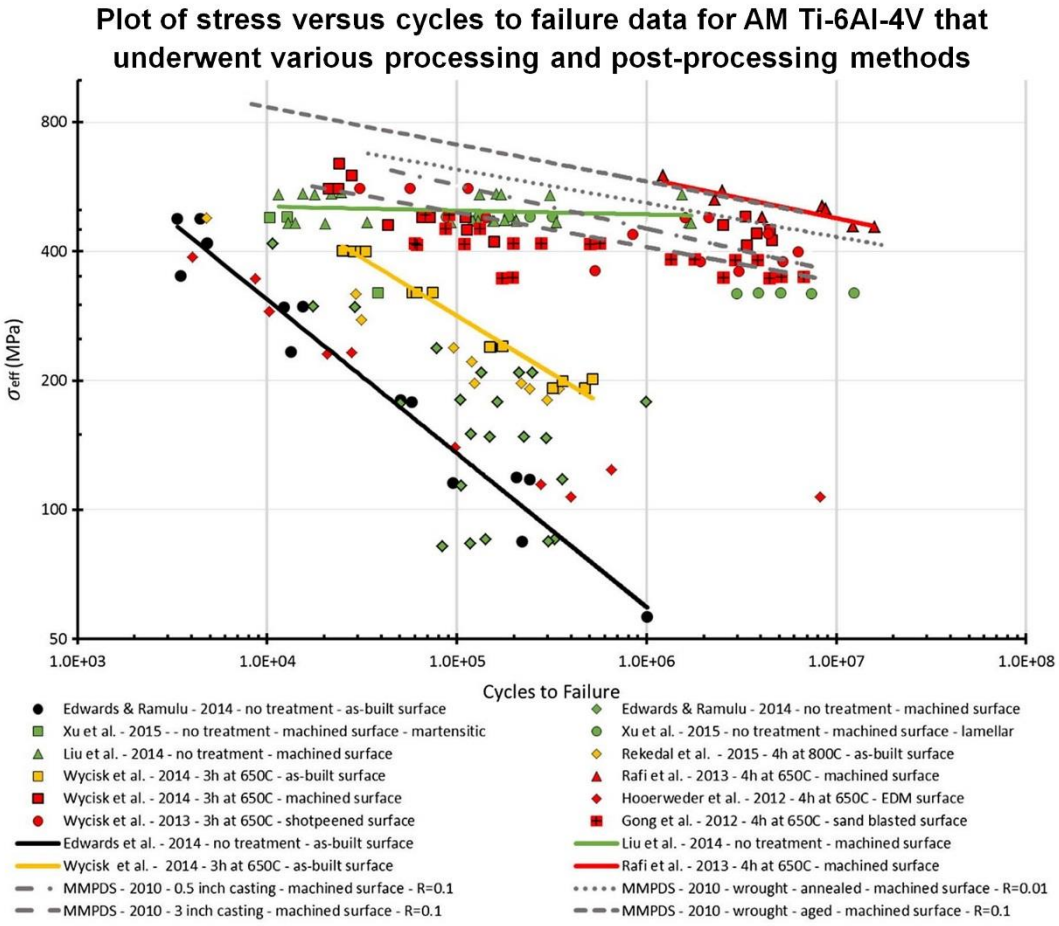

Figure 9. Fatigue test results compiled by [130] shows the effect of various post-processing treatments on improving the fatigue properties of AM-processed Ti-6Al-4V.

To sum up**,** it can be concluded that anisotropy in mechanical properties was indeed exhibited in metal AM parts. Nevertheless, some parts fabricated from certain metal AM systems could exhibit less anisotropy. This is due to the differences in processing variables that lead to a more homogenous microstructure and residual stress distribution. Moreover, it is important to note that post-processing such as surface machining and heat treatment can effectively improve the comprehensive mechanical properties of metal AM parts to be comparable and even superior to their cast and wrought equivalents.

Table 5. Summary of fatigue properties of PBF metal AM Ti-6Al-4V parts and ASTM wrought Ti-6Al-4V.

Material	Condition	Process	Test Orientation	Load Ratio (R)	Anisotropy in fatigue overload (%)	Fatigue overload (MPa √m)	Cycles (m/cycle)	Paris Slope	Anisotropy in fatigue threshold (%)	Threshold (MPa √m)	Ref.
Electron beam based											
Ti-6Al-4V	As-built	Arcam A2	Horizontal (X-Z,X-Y)	0.1,0.3, 0.7	28.1	63-96		1.4-3.1	33.3	3.5-5.7	[24]
			Vertical (Z-X)	0.3		69		2.6		3.8	
Ti-6Al-4V	As-built	MTT 250	Horizontal (X-Y)		32.7	33.3	1.2×10^{7}	2.61	7.9	6.3	[125]
			Vertical (X-Z,Y-Z)			22.4-36.0	1.7×10^{7}-2.1×10^{7}	2.37-2.45		5.8-5.9	
Laser beam based											
Ti-6Al-4V	As-built	SLM	Horizontal (X-Y-B)				5.79×10^{12}	3.37			[80]
	As-built	SLM	Vertical (X-Z-E,Z-X-M)				2.08×10^{12} - 7.51×10^{12}	4.17-4.41			
Ti-6Al-4V	SR	SLM	Horizontal (X-Y-B)				9.93×10^{15}	5.84			[80]
	SR	SLM	Vertical (X-Z-E,Z-X-M)				1.16×10^{11} - 8.85×10^{12}	3.24-3.35			
Ti-6Al-4V	HT	SLM	Horizontal (X-Y-B)				2.04×10^{12}	3.83			[80]
	HT	SLM	Vertical (X-Z-E,Z-X-M)				1.71×10^{11}-2.58×10^{11}	3.11-3.35			
Ti-6Al-4V		Wrought								2.3-4.2	[131, 132]

4. Heterogeneity in metal AM

Given that one of the main advantages of AM is its ability to directly manufacture complex geometries, understanding the heterogeneity that exists in metal AM parts is equally important as the anisotropy [20]. A comprehensive set of materials data base would allow designers better utilize metal AM technologies for more demanding end-use applications [133].

Microstructural heterogeneity of metal AM parts can arise from differences in morphology, size, orientation, and chemical composition of phases and grains. Such differences were resulted from the varying thermal conditions (e.g. thermal gradient and cooling rate) that were included in different metal AM processes [26, 134, 135].

4.1 Heterogeneity in microstructure

4.1.1 Phase constitution

Difference in phase constitution is an important source of microstructural heterogeneity in metal AM parts. For example, in the case of α+β titanium alloys (Ti-6Al-4V), three phases were often reported, i.e. α phase, β phase and α′ martensitic phase [85]. Due to the complex phase transformation processes [136], it is difficult to predict the phase constitution in AM titanium alloys accurately. A thorough study has recently described a complete phase transformation sequence that Ti-6AL-4V underwent during EBM process [136, 137]. It was reported that the cooling rate and build temperature were the two key process conditions to influence the final phase constitutions in the metal AM parts [136]. The proposed phase transformation sequence provides a glimpse of the relationship between the complex thermal history of the EBM process and the final microstructure obtained. A study on SLM-built Ti-6Al-4V has also shown microstructural variation along the build direction [138]. It was suggested that the microstructural variations were caused by a cyclic thermal history from successive depositions. Moreover, the top region only exhibited α′ martensitic phase that indicated the as-deposited condition without phase decomposition [138]. Likewise, for the CoCr alloys processed with EBM, the elevated build temperature caused the metastable γ-face centered cubic (fcc) phase transform to the stable ε-hexagonal closed packed (hcp) phase during the build process [139, 140], resulting in microstructural heterogeneity along the build direction as shown in Figure 10 [139].

A study regarding the build thickness dependent microstructure and mechanical properties of EBM-built Ti-6Al-4V have reported that the phase constitution highly relied on the cross-sectional area of the metal AM part [134]. Microstructure of thin cross-sectional area would have a phase constitution that predominantly consists of brittle martensitic phase while it would be ductile α+β dual phase for thick cross-sectional area [134]. This is due to the fact that the thick cross sectional area could retain a higher temperature with to lower cooling rates [134, 141]. Another study based on DED-built IN718 superalloy has also attributed the formation of precipitates to cause heterogeneity in hardness [13]. Microstructural heterogeneity

was thought to be due to solidification segregation, with the presence of niobium along the grain boundary promoting the heterogeneous nucleation and growth of γ″ phase [13]. Thus, it can be seen that the varying phase constitution at different locations for varying geometry may induce heterogeneity in metal AM parts.

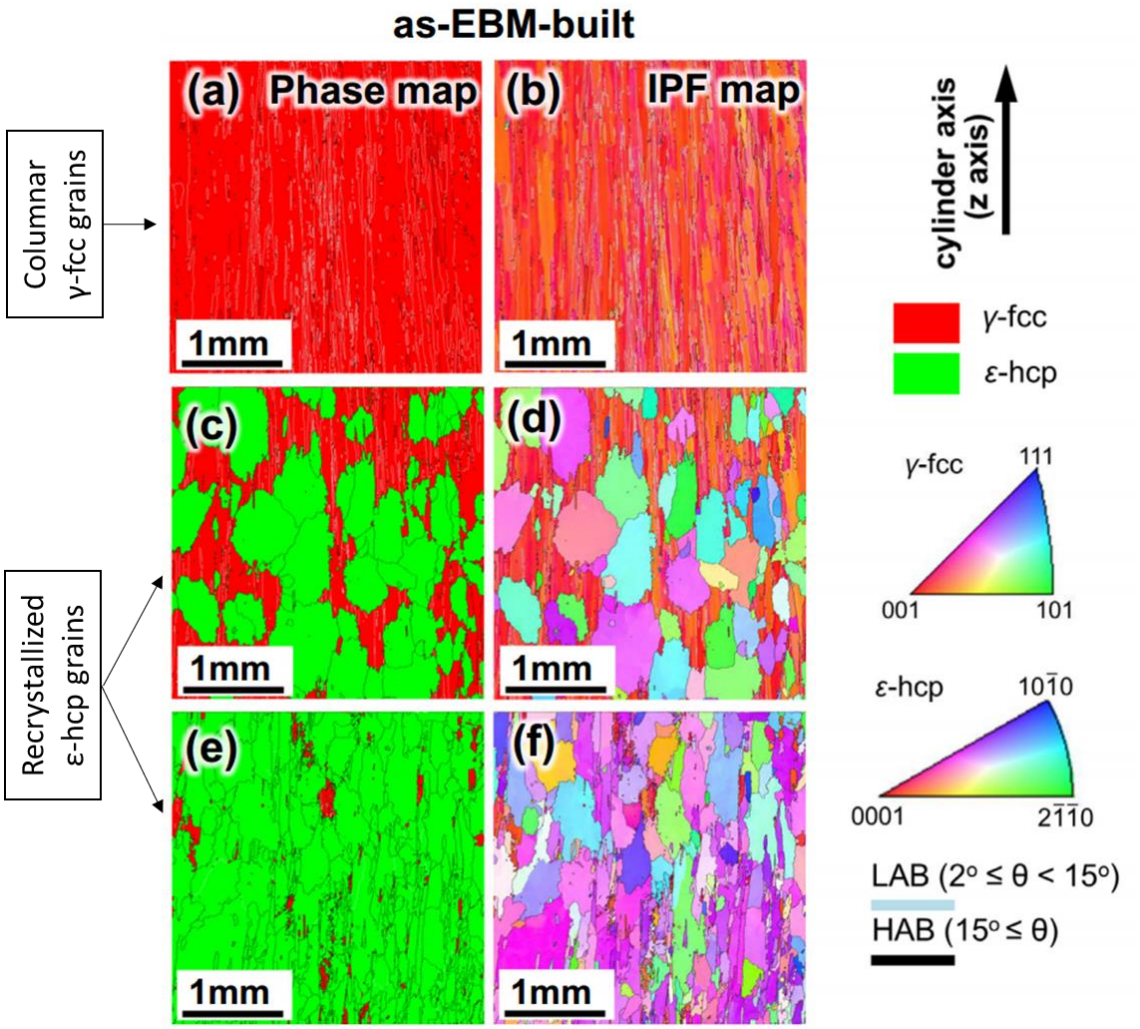

Figure 10. EBSD phase map (a, c, e) and IPF crystallographic orientation map (b, d, f) on the longitudinal cross-section of EBM-built CoCrMo showing variation in phase composition and grain morphology [140].

4.1.2 Layer banding and microstructure coarsening

Layer bandings is a popular observed phenomenon in metal AM materials [26, 44, 142, 143]. Prior research has shown that in titanium alloys, layer banding was a result of segregation of vanadium and aluminium. However, a study by Kelly & Kampe revealed no systematic elemental variation in DED-built Ti-6Al-4V [142], and concluded that such layer bands were

resulted from the cyclic thermal history that the part experienced after multiple layers' deposition [26, 143]. A study on wire-fed DED-built Ti-6Al-4V developed a schematic diagram showing the formation of the layer bands as shown in Figure 11 [142]. Differences in the microstructure feature (e.g. mean width of α laths) could be clearly observed between the top and the bottom of a layer band [142]. Despite the unique microstructural morphology, it is still unclear how such heterogeneity affects Ti-6Al-4V AM parts' mechanical properties. Another study conducted by Nakano *et al.* also reported the layer band in EBM-built Ti-48Al-2Nb-Cr alloy and also concluded that this layer bands was resulted from cyclic thermal history. Moreover, this layer band improves the ductility of Ti-48Al-2Nb-Cr alloy in a certain loading direction [42].

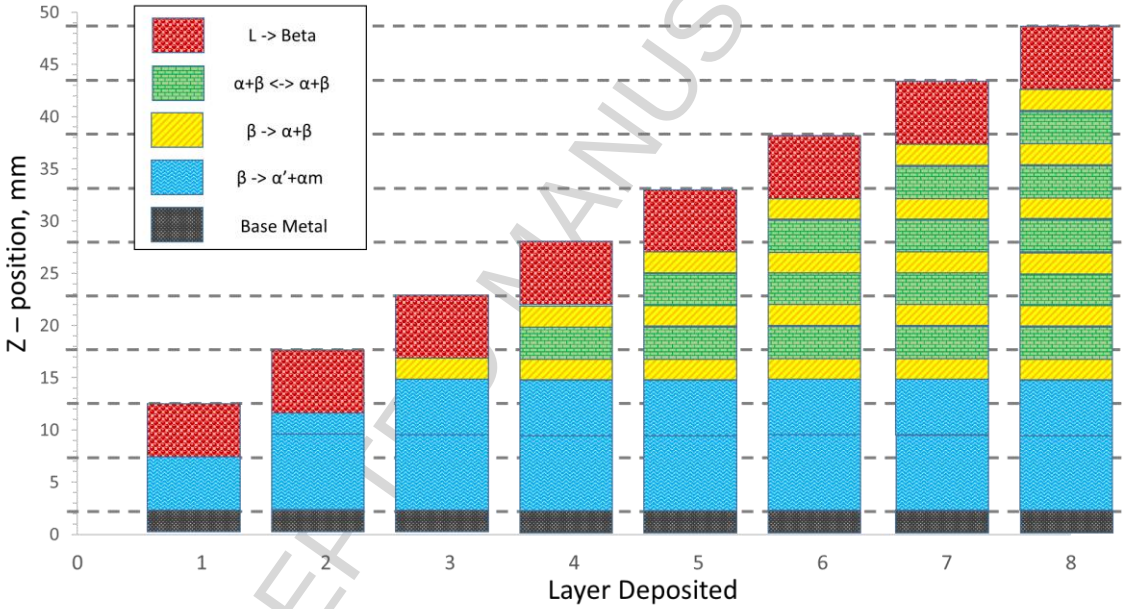

Figure 11. Microstructural evolution map of the build as each layer is deposited (reproduced from [26, 142]) showing the formation of the layer banding microstructure in DED Ti-6Al-4V.

4.1.3 Grain Morphology

The grain morphology within metal AM parts has been shown to depend on the process parameters and materials [67, 72, 84, 144, 145]. Studies on EBM-built IN718 has shown that site specific control of the grain morphology by varying the processing parameters (e.g. line offset, speed function) was possible with metal AM [72, 144]. Heterogeneity in grain

morphology was also observed in EBM-built CoCr parts, due to recrystallization caused by the high build temperature [140]. While in EBM-built Ti-6Al-4V parts, the increase in columnar grain width was observed with the increased build height [84]. Additionally, an equiaxed-to-columnar transition of prior β grains in Ti-6Al-6V was reported at the start of the EBM build as shown in Figure 12 [84]. It was suggested in the study that the higher heat conductivity of the start plate material resulted in a higher degree of super cooling which led to the transition of grain morphology [84].

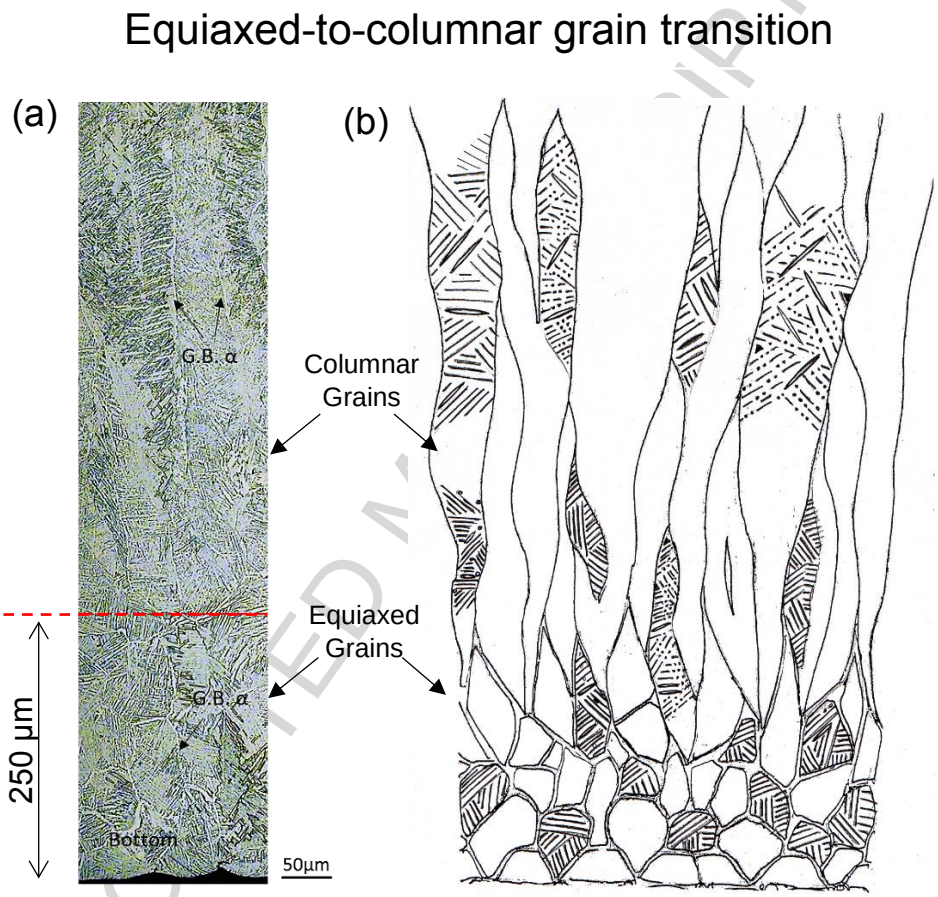

Figure 12. (a) OM micrograph and (b) schematic showing the equiaxed-to-columnar transition of prior β grains in EBM-built Ti-6Al-4V [84].

4.1.4 Microstructural feature size

Several studies have shown that the microstructure of AM-processed Ti-6Al-4V tended to become finer at the top region as compared to the bottom [146-148]. While other studies showed opposite trends instead [11, 84]. Microstructural scale is known to decrease with increasing cooling rate [149]. There are three main paths that heat was lost in the metal AM process (1) radially through the surrounding powder bed or environment, (2) vertically

downwards through the build start plate via conduction and (3) vertically upwards from the top layer via convection and/or radiation towards the ambient [15, 141]. At the very top region of the metal AM parts, the fine microstructure is likely due to the high cooling rate induced by heat loss of convection and radiation and the lack of remelting and thermal cycling that prior layers experienced [142]. Additionally, microstructural scale was found to be dependent on cross-sectional thickness due to differences in the hatch lengths and thermal mass as can be observed in Figure 13 [141, 150, 151]. Coarse microstructure size could be observed in the thick cross-sectional parts due to the slow cooling rates within high thermal mass [134]. A study have also shown that it is possible to induce refinement of microstructure through the use of in-situ printed heat sinks in EBM-built Ti-6Al-4V [152].

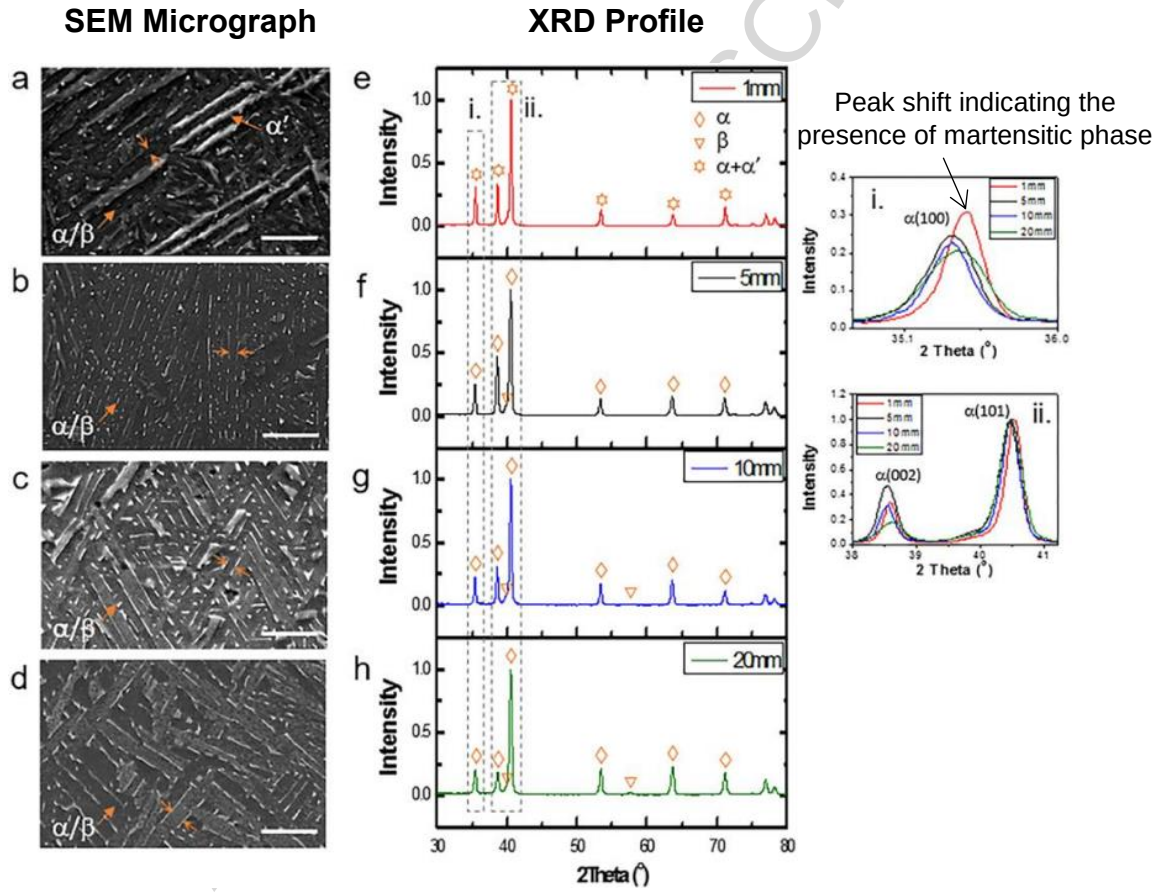

Figure 13. SEM images showing the microstructure size with increasing cross-sectional thickness with their respective XRD profiles (a,e) 1mm, (b,f) 5mm, (c,g) 10mm and (d,h) 20 mm [136] showing the heterogeneous microstructures in EBM-built Ti-6Al-4V.

4.1.5 Processing deficiency

AM processing defects have been reported to contribute to anisotropy in mechanical properties of metal AM parts such as fracture toughness and tensile strength [9, 101].

Additionally, there have also been studies reported that such defects were not homogenously distributed within the build as shown in Figure 14a and b [23]. Unfortunately, the mechanism for the formation of location specific defects is not well understood yet [153]. The spherical pore defects with a diameter of 10-50 µm were reported to be due to the trapped gas pore in gas atomized powders [135, 137, 154]. A study has also shown that such trapped gas porosity decreased with decreasing speed function parameter of EBM, possibly by allowing more time for the trapped gas to escape from the slowly moved melt pool [154]. Other processing defects such as un-melted powder and layer gaps can also occur during the AM process. HIP treatment has shown to be able to reduce the amount of such processing defects effectively [9]. Figure 14c shows that the defect density has a significant effect on the fracture toughness of the metal AM part [23].

A study on a SL process reported that defect distribution within the aluminium alloy sample was not homogenous [14]. A point to note from the study was that region where cracks originate did not correspond to the location of voids. Instead, it attributed the mechanism of the formation of the cracks to the strain localization caused by the high strain rate deformation induced from the rotating sonotrode that was used to fuse the metal sheets together [14].

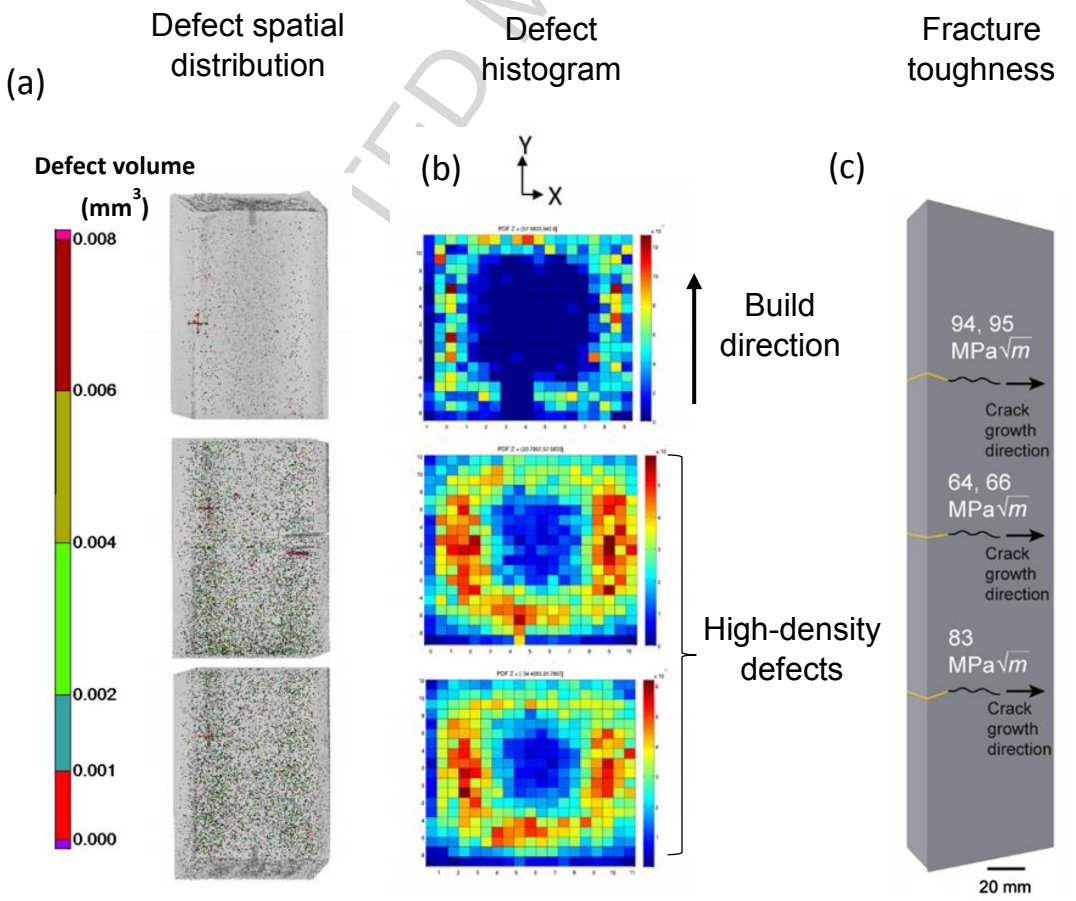

Figure 14. (a) µCT scans showing defects spatial distribution in EBM-built Ti-6Al-4V (b) defect histogram for the EBM-built Ti-6Al-4V at bottom, middle and top region (c) fracture toughness variation at the bottom, middle and top region respectively [23] showing the heterogeneity in fracture toughness correlates with the defect density.

4.1.6 Heterogeneous recrystallization

Post heat treatment is a common method to homogenize the microstructure of the as-deposited metal AM part [100, 101]. Figure 15a shows a schematic of how vacuum annealing treatment can induce homogenous grain recrystallization within SLM-built iron part [155]. However, a study has reported that partial recrystallization in heat treated SLM-built IN718 resulted in a heterogeneous grain structure as shown in Figure 15 [156] instead. It was suggested that heterogeneous residual stresses within the metal AM parts may account for such partial recrystallization [20]. Moreover, homogeneous grains sizes (~500-3000 µm) were found in DED-built Ti-6Al-4V after post heat treatment [157]. Of note is that such post-processing procedures for metal AM parts may have to take into account of both the materials and manufacturing techniques.

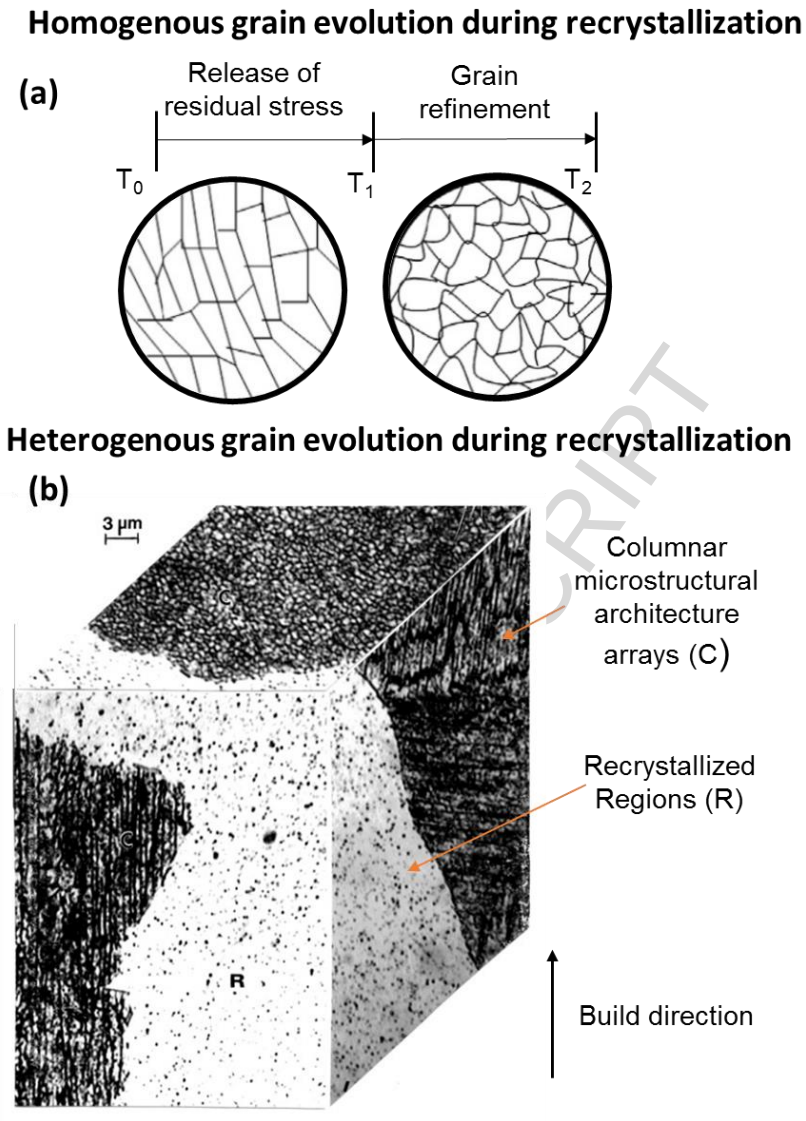

Figure 15. (a) Schematic diagram of typical homogenous grain evolution during the grain recrystallization phenomenon [155]. (b) 3D Optical Micrograph (OM) composite view of the SLM-built IN718 microstructure [156] showing the heterogeneity in microstructure caused by heterogeneous recrystallization.

4.2 Heterogeneity in mechanical properties

4.2.1 Tensile properties

Table 6 lists the differences in tensile strength along the build direction of the AM Ti-6Al-4V by various studies [10, 11, 84, 99, 158-161]. Higher tensile properties were reported in the lower half of the block samples as compared to the upper half, which was attributed to oxygen strengthening and finer microstructure [10, 11]. The tensile strength of Ti-6Al-4V parts typically increases with increasing oxygen content and finer microstructure [112, 162]. Furthermore, a study on EBM-built Ti-6Al-4V also reported an increase in strain hardening effect with increasing built height due to lesser annealing [84].

Table 6. Summary of tensile properties of various metal AM parts.

Material	Condition	Process	Position	Yield Strength (MPa)	Ultimate Tensile Strength (MPa)	Elongation (%)	Ref.
Ti-6Al-4V	Machined	DED	Upper half	945	1041	14.5	[10]
			Lower half	970	1087	13.6	
Ti-6Al-4V	Machined	EBM	Upper half	859.3	942.4	18.8 ± 2.5	[11, 99]
			Lower half	898.9	976.6	17.9 ± 0.7	
Ti-6Al-4V ELI	Machined	EBM	Upper half	823-827	940-944	13.2	[84]
			Lower half	836-851	953-964	16.3	
Ti-6Al-4V ELI	Machined	EBM	Upper half	903.6 ± 24.6	991.8 ± 21.7	16.4 ± 0.8	[158]
			Lower half	911.9 ± 34.3	995.5 ± 28.5	13.5 ± 0.4	
Ti-6Al-4V ELI	Machined	EBM	Upper half	986.5	1050.5	14.3	[159]
			Lower half	987.5	1056.5	12.7	
Ti-6Al-4V	Machined	EBM	Upper half	991.1 ± 9.3	1065.9 ± 10.2	14.6 ± 0.1	[160]
			Lower half	990.9 ± 22.5	1056± 24.2	16.7 ± 1.0	
Ti-6Al-4V	Machined	DMLS	Upper half	1059	1221	4.8	[161]
			Lower half	~1167	~1281	~2.6	

4.2.2 Hardness

Hardness testing is an effective method to characterize the localized mechanical strength of metal AM parts. Table 7 summarised of hardness properties of various AM metal alloys. A recent study has shown that Vickers microhardness correlated well with the microstructural features of AM titanium alloy and it obeyed the Hall-Petch's relationship [134]. Studies have been carried out to investigate the effect of cross-sectional area on hardness values [15, 83, 134]. An earlier study reported that the effect of metal AM part size on the microhardness was little, possibly due to the insufficient thermal isolation between them [83]. While a recent study reported that hardness property was dependent on cross-sectional area [15, 134, 141]. It was shown that with increasing cross-sectional area, the microhardness was decreased due to microstructural coarsening [15, 40, 90, 134, 141]. The rationale for the microstructural coarsening is due to greater thermal input and slower cooling rates experienced by the part with the thicker cross-sectional area [15, 141]. The study also showed that differences in the 2D-planar geometry had an influence on the microhardness as well due to differences in heat flux. Studies have also been conducted on the effect of built height on the hardness [15, 83, 84]. However, such studies showed conflicting results. For example, a study by Hrabe *et al.* [83] reported no significant differences in Vickers microhardness values up to 25 mm from the substrate while the study from Tan *et al*. [84] showed that there were differences in the Vickers microhardness values with build height.

Tan *et al*. reported that Vickers microhardness decreased in value with increasing build height in EBM-built Ti-6Al-4V [84]. It was suggested that due to the higher cooling rate induced by the higher thermal conductivity of the stainless steel substrate. The microstructure at the bottom region was finer as compared to the top region. However, Wang *et al.* systematically examined the microhardness within an impeller component [15]. The study reported that microhardness value was increased with increasing build height. It must be noted that the part in Wang *et al*. work had a decreasing cross-sectional area with increasing build height. The difference in cross-sectional area may contribute to that result.

Many studies have thus concluded that heterogeneity in hardness values was dependent on the thermal input experience by the specific layer. A larger cross-sectional area would result in a higher thermal input as compared to a smaller cross-sectional area, resulting in different final microstructures. Future improvement on varying the process parameters with regards to the cross-sectional area could help alleviate such heterogeneity in hardness.

Table 7. Summary of hardness properties of various metal AM parts.

Material	Process/Model	Microhardness (Hv)	Distance Measured from the substrate (mm)	Ref.
Ti-6Al-4V	EBM/Arcam S400	~460-360	~68	[146]
Ti-6Al-4V	EBM/Arcam S12	347	2-25	[83]
Ti-6Al-4V ELI	EBM/Arcam A2XX	319±5-327±5	24	[84]
Ti-6Al-4V	EBM/Arcam A2X	343-365	4-35	[15]
Ti-6Al-4V	EBM/Arcam A2X	380	0-4.5	[43]
Ti-6Al-4V ELI	EBM/Arcam A2	~368	0-110	[159]
Ti-6Al-4V	EBM/Arcam A2X	~340	~13	[11]
Pure Cu	EBM/Arcam A2	57-88	N.A.	[163]
AlCoCrFeNi	EBM/Arcam A2X	400-500	0-16	[164]
SS316L	EBM/Arcam S12	184 ± 11	2	[165]
IN718	EBM/Arcam S12	241 ± 12	2	[165]
Al-8.5Fe-1.3V-1.7Si	EBM/Arcam A2X	153 ± 2.5	N.A.	[166]
Ti-6Al-4V	SLM/ Concept Laser M2	360	N.A.	[167]
SS316L	SLM/SLM 250 HL	213-220	N.A.	[47]
IN718	SLM/LSNF-I	365	1.3-2.4	[168]
Al-8.5Fe-1.3V-1.7Si	SLM/DEYU LM 200 SLM	135-175	N.A.	[169]

4.2.3 Fracture toughness

Location dependence in fracture toughness has been observed in EBM-built Ti-6Al-4V due to the heterogeneity in the microstructure and defect distribution [9]. A related study also performed HIP process to investigate its effect on the heterogeneity in fracture toughness [23]. However, the measured fracture toughness was found to be lesser due to coarsening of the microstructure after the HIP process and the heterogeneity observed was not eliminated.

In summary, it can be deduced that anisotropy and heterogeneity in the mechanical properties of metal AM parts are due to the anisotropic and heterogeneous microstructure and material properties. Despite the anisotropy and heterogeneity in the mechanical properties, it can be concluded that the mechanical properties of post-processed metal AM parts are

equivalent or better as compared to their cast equivalent. Further improvement regarding the optimization of heat treatment process parameters is highly demanded to produce end-use parts with fine microstructure in order to approach the static and dynamic mechanical properties of their wrought equivalent.

5. Modelling on anisotropy and heterogeneity

Numerical modelling of the thermal conditions of AM processes allows a better understanding of the anisotropic and heterogeneous microstructure which determines the final mechanical properties. An early study has developed a thermos-kinetic model of multilayer laser-based powder deposition, coupled FE heat transfer calculations, phase transformation data, and microstructure-property relationships, showing the increase in Vickers hardness with increasing build height and with minimizing substrate size [170]. Numerical modelling has also been used to simulate beam power-velocity (P-V) process maps and solidification maps in an effort to control the microstructure for various metal AM processes as shown earlier in Figure 5c and d.

Other studies have also developed heat transfer and microstructural evolution equations for EBM-built Ti-6Al-4V showing that the heat transfer arising from the selective melting was sufficient to induce microstructure evolution through several layers below. Figure 16 shows an FEM model of the temperature variation of metal AM parts with varying thicknesses along the build height and the evolution of volume fraction of α phase due to the variations in the temperature field within the metal AM part [134, 171]. It provides a firm support to experimental works regarding the phase constitution and microstructural coarsening [142, 171].

A recent study has also developed a model that was capable of calculating fraction, morphology and size of phases, with a measured or modelled thermal history in AM-processed Ti-6Al-4V [172]. With the more research focusing on modelling metal AM processes, a better understanding of the interrelationship between process-microstructure-mechanical properties can be achieved.

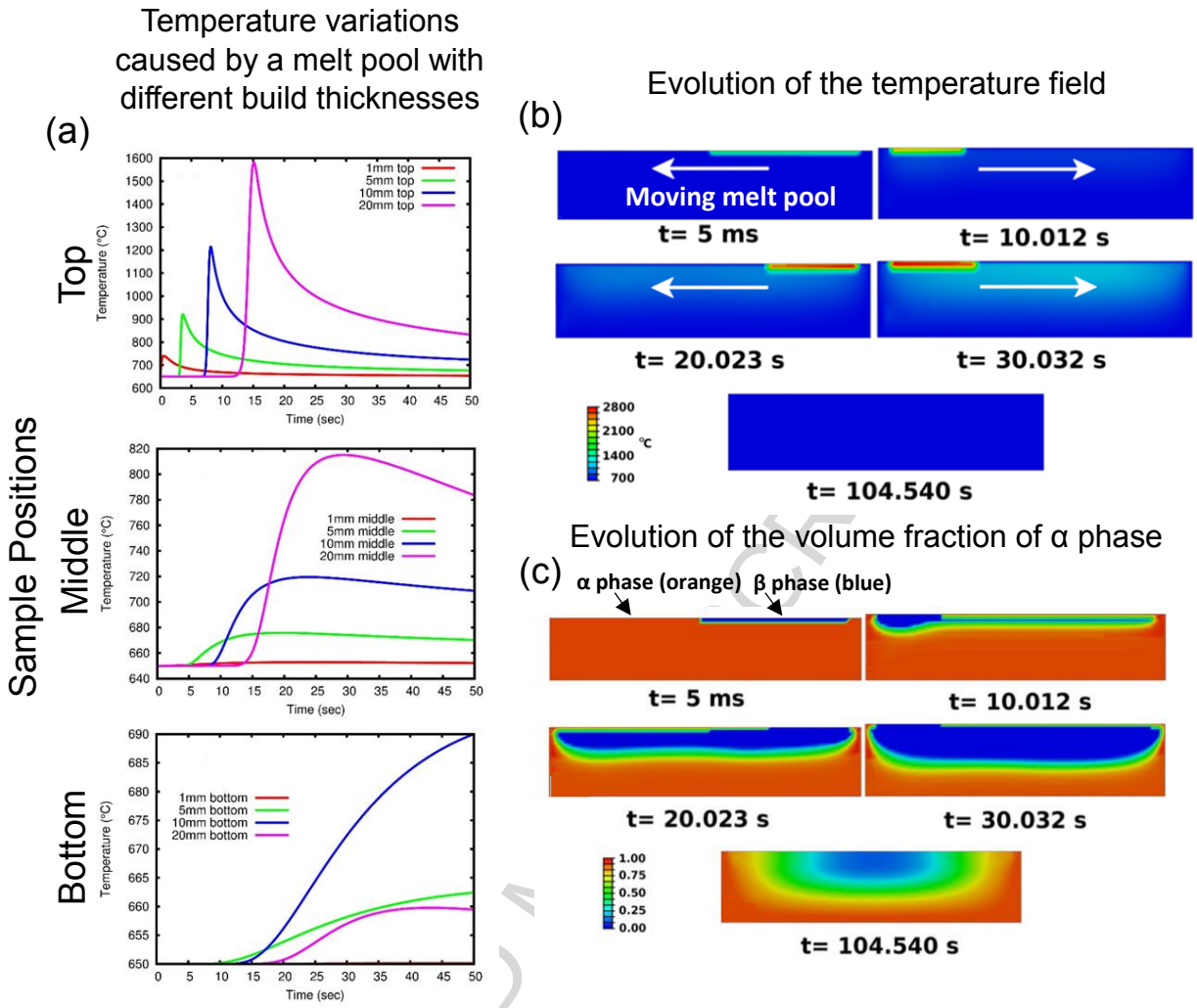

Figure 16. Temperature evolution curves with respect to time for the positions of (a) top, (b) middle, and (c) bottom of the sample. Evolution of the (d) temperature field and (e) volume fraction of α phase after deposition of 4 layers of powder [134, 171] showing the possibility of using numerical simulations to model the anisotropic and heterogenous microstructure that is formed in metal AM parts.

Concluding remarks

Metal AM became a competitive manufacturing process to conventional manufacturing techniques such as machining and casting with regards to the fabrication of components with complex geometries out of hard to process materials (e.g. titanium alloys). Metal AM processes could be broadly categorized as powder-bed fusion (PBF), directed energy deposition (DED) and sheet lamination (SL). During the layer-by-layer fabrication, the metallic part was subjected to processing variables such as deposition rate, beam power, build environment and

processing temperature which have an influence towards its final microstructure and mechanical properties. In general, despite the reported anisotropy and heterogeneity, the quasi-static mechanical properties (e.g. tensile strength and hardness) of metal AM parts often could meet the minimum requirements in comparison with their cast and wrought equivalents. However, post processing of metal AM parts must be implemented to obtain comparable dynamic mechanical properties (e.g. fatigue properties) as conventionally produced parts. Such post processing techniques are currently a costly means to control the anisotropic and heterogeneous microstructure within metal AM parts.

It can be deduced via the published datum summarized in this article, that the cause for the anisotropic and heterogeneous microstructure and mechanical properties of metal AM parts was due to either microstructural features or defects. The influencing factors for the anisotropy and heterogeneity in the microstructure include: (1) grain morphology; (2) crystallographic texture; (3) lack-of-fusion defects; (4) phase transformation; (5) heterogeneous recrystallization; (6) layer banding and (7) microstructural coarsening. These factors were systematically discussed in terms of the processing variables within the metal AM process. Given the current state-of-the-art in metal AM, it is difficult to vary the processing variables in-situ with respect to a part's geometry and size so as to control its microstructure. However, with continued development in this technology, it is likely that better control over the processing variables during the fabrication process can be achieved.

Literatures have shown that microstructural modification of AM metallic materials can be achieved via the use of a roller mechanism that applied a load after each deposited layer or through the use of in-situ printed heat sink. Traditionally, adjusting the build orientation and specifying a minimum cross-sectional thickness were ways to reduce the effect of the anisotropy and heterogeneity in material properties. Moreover, it was widely shown that horizontally orientated AM parts typically had a higher mechanical strength as compared to vertically orientated ones. As such if the build part is horizontally orientated along the load direction and that fine geometrical features are scaled up to increase mechanical strength, the anisotropy and heterogeneity might be effectively minimised or even eliminated.

Acknowledgements

The authors are grateful for financial support provided by A*STAR Industrial Additive Manufacturing Program: Work Package 3 (Electron Beam Melting, Grant No. 1325504103). We also acknowledge the financial support from Singapore Centre for 3D Printing funded by the National Research Foundation.

References

[1] C.K. Chua, K.F. Leong, 3D printing and additive manufacturing: principles and applications, 2015.

[2] I. Gibson, D.W. Rosen, B. Stucker, Additive manufacturing technologies, Springer2010.

[3] J.D. Strickland, Applications of Additive Manufacturing in the Marine Industry, Proceedings of PRADS2016 4 (2016) 8th.

[4] N. Patil, D. Pal, B. Stucker, A new finite element solver using numerical Eigen modes for fast simulation of additive manufacturing processes, Proceedings of the Solid Freeform Fabrication Symposium, Austin, TX, Aug, 2013, pp. 12-14.

[5] X.P. Tan, Y.J. Tan, C.S.L. Chow, S.B. Tor, W.Y. Yeong, Metallic powder-bed based 3D printing of cellular scaffolds for orthopaedic implants: A state-of-the-art review on manufacturing, topological design, mechanical properties and biocompatibility, Materials Science and Engineering: C (2017) 76: 1328-1343.

[6] T. Wohlers, Wohlers report 2016, Wohlers Associates, Inc2016.

[7] K. Vartanian, T. McDonald, Accelerating Industrial Adoption of Metal Additive Manufacturing Technology, JOM 68(3) (2016) 806-810.

[8] C.Y. Yap, C.K. Chua, Z.L. Dong, Z.H. Liu, D.Q. Zhang, L.E. Loh, S.L. Sing, Review of selective laser melting: Materials and applications, Applied Physics Reviews 2(4) (2015) 041101.

[9] J.J. Lewandowski, M. Seifi, Metal Additive Manufacturing: A Review of Mechanical Properties, Annual Review of Materials Research 46(1) (2016) 151-186.

[10] B.E. Carroll, T.A. Palmer, A.M. Beese, Anisotropic tensile behavior of Ti–6Al–4V components fabricated with directed energy deposition additive manufacturing, Acta Materialia 87 (2015) 309-320.

[11] P. Wang, M.L.S. Nai, X. Tan, W.J. Sin, S.B. Tor, J. Wei, Anisotropic Mechanical Properties in a Big-Sized Ti-6Al-4V Plate Fabricated by Electron Beam Melting, TMS 2016 145th Annual Meeting & Exhibition: Supplemental Proceedings, Springer International Publishing, Cham, 2016, pp. 5-12.

[12] Z. Wang, T.A. Palmer, A.M. Beese, Effect of processing parameters on microstructure and tensile properties of austenitic stainless steel 304L made by directed energy deposition additive manufacturing, Acta Materialia 110 (2016) 226-235.

[13] Y. Tian, D. McAllister, H. Colijn, M. Mills, D. Farson, M. Nordin, S. Babu, Rationalization of Microstructure Heterogeneity in INCONEL 718 Builds Made by the Direct Laser Additive Manufacturing Process, Metallurgical and Materials Transactions A 45(10) (2014) 4470-4483.

[14] N. Sridharan, M. Gussev, R. Seibert, C. Parish, M. Norfolk, K. Terrani, S.S. Babu, Rationalization of anisotropic mechanical properties of Al-6061 fabricated using ultrasonic additive manufacturing, Acta Materialia 117 (2016) 228-237.

[15] P. Wang, X. Tan, M.L.S. Nai, S.B. Tor, J. Wei, Spatial and geometrical-based characterization of microstructure and microhardness for an electron beam melted Ti–6Al–4V component, Materials & Design 95 (2016) 287-295.

[16] Y. Zhu, X. Tian, J. Li, H. Wang, The anisotropy of laser melting deposition additive manufacturing Ti–6.5Al–3.5Mo–1.5Zr–0.3Si titanium alloy, Materials & Design 67 (2015) 538-542.

[17] R.R. Dehoff, C. Tallman, C.E. Duty, W.H. Peter, Y. Yamamoto, W. Chen, C.A. Blue, Case study: additive manufacturing of aerospace brackets, Advanced Materials and Processes 171(3) (2013).

[18] J.K. Patel, B. Wilshire, The challenge to produce consistent mechanical properties in Nb-HSLA strip steels, Journal of Materials Processing Technology 120(1–3) (2002) 316-321.

[19] J.J. Sobczak, L. Drenchev, Metallic Functionally Graded Materials: A Specific Class of Advanced Composites, Journal of Materials Science & Technology 29(4) (2013) 297-316.

[20] W.J. Sames, F.A. List, S. Pannala, R.R. Dehoff, S.S. Babu, The metallurgy and processing science of metal additive manufacturing, International Materials Reviews 61(5) (2016) 315-360.

[21] W.E. Frazier, Metal Additive Manufacturing: A Review, Journal of Materials Engineering and Performance 23(6) (2014) 1917-1928.

[22] S.L. Sing, J. An, W.Y. Yeong, F.E. Wiria, Laser and electron-beam powder-bed additive manufacturing of metallic implants: A review on processes, materials and designs, Journal of Orthopaedic Research 34(3) (2016) 369-385.

[23] M. Seifi, A. Salem, D. Satko, J. Shaffer, J.J. Lewandowski, Defect distribution and microstructure heterogeneity effects on fracture resistance and fatigue behavior of EBM Ti–6Al–4V, International Journal of Fatigue 94, Part 2 (2017) 263-287.

[24] M. Seifi, M. Dahar, R. Aman, O. Harrysson, J. Beuth, J.J. Lewandowski, Evaluation of Orientation Dependence of Fracture Toughness and Fatigue Crack Propagation Behavior of As-Deposited ARCAM EBM Ti-6Al-4V, JOM 67(3) (2015) 597-607.

[25] A. Basak, S. Das, Epitaxy and Microstructure Evolution in Metal Additive Manufacturing, Annual Review of Materials Research (2016).

[26] S.M. Kelly, S.L. Kampe, Microstructural evolution in laser-deposited multilayer Ti-6Al-4V builds: Part II. Thermal modeling, Metallurgical and Materials Transactions A 35(6) (2004) 1869-1879.

[27] M.-W. Wu, P.-H. Lai, J.-K. Chen, Anisotropy in the impact toughness of selective laser melted Ti–6Al–4V alloy, Materials Science and Engineering: A 650 (2016) 295-299.

[28] B. Zhang, X. Lee, J. Bai, J. Guo, P. Wang, C.-n. Sun, M.L. Nai, G. Qi, J. Wei, Study of selective laser melting (SLM) Inconel 718 part surface improvement by electrochemical polishing, Materials & Design 116 (2017) 531-537.

[29] ASTM, Standard Terminology for Additive Manufacturing Technologies, ASTM F2792-12a, ASTM International, West Conshohocken, PA, 2010.

[30] H. Bikas, P. Stavropoulos, G. Chryssolouris, Additive manufacturing methods and modelling approaches: a critical review, The International Journal of Advanced Manufacturing Technology 83(1) (2016) 389-405.

[31] M.F. Zäh, S. Lutzmann, Modelling and simulation of electron beam melting, Production Engineering 4(1) (2010) 15-23.

[32] S.M. Thompson, L. Bian, N. Shamsaei, A. Yadollahi, An overview of Direct Laser Deposition for additive manufacturing; Part I: Transport phenomena, modeling and diagnostics, Additive Manufacturing 8 (2015) 36-62.

[33] K.P. Karunakaran, S. Suryakumar, V. Pushpa, S. Akula, Low cost integration of additive and subtractive processes for hybrid layered manufacturing, Robotics and Computer-Integrated Manufacturing 26(5) (2010) 490-499.

[34] M. Hedges, N. Calder, Near-Net-Shape Rapid Manufacture and Repair by LENS®, Rapid Prototyping 12(4) (2006) 1.

[35] P. Muller, P. Mognol, J.-Y. Hascoet, Modeling and control of a direct laser powder deposition process for Functionally Graded Materials (FGM) parts manufacturing, Journal of Materials Processing Technology 213(5) (2013) 685-692.

[36] R.R. Dehoff, S.S. Babu, Characterization of interfacial microstructures in 3003 aluminum alloy blocks fabricated by ultrasonic additive manufacturing, Acta Materialia 58(13) (2010) 4305-4315.

[37] R.J. Friel, R.A. Harris, Ultrasonic Additive Manufacturing – A Hybrid Production Process for Novel Functional Products, Procedia CIRP 6 (2013) 35-40.

[38] X.P. Tan, P. Wang, Y. Kok, W.Q. Toh, Z. Sun, S.M.L. Nai, M. Descoins, D. Mangelinck, E. Liu, S.B. Tor, Carbide precipitation characteristics in additive manufacturing of Co-Cr-Mo alloy via selective election beam melting, Scripta Materialia 143 (2018) 117-121.

[39] Y. Kok, X. Tan, S.B. Tor, C.K. Chua, Fabrication and microstructural characterisation of additive manufactured Ti-6Al-4V parts by electron beam melting, Virtual and Physical Prototyping 10(1) (2015) 13-21.

[40] J.K. Algardh, T. Horn, H. West, R. Aman, A. Snis, H. Engqvist, J. Lausmaa, O. Harrysson, Thickness dependency of mechanical properties for thin-walled titanium parts manufactured by Electron Beam Melting (EBM)®, Additive Manufacturing 12, Part A (2016) 45-50.

[41] P. Wang, W. Sin, M. Nai, J. Wei, Effects of Processing Parameters on Surface Roughness of Additive Manufactured Ti-6Al-4V via Electron Beam Melting, Materials 10(10) (2017) 1121.

[42] M. Todai, T. Nakano, T. Liu, H.Y. Yasuda, K. Hagihara, K. Cho, M. Ueda, M. Takeyama, Effect of building direction on the microstructure and tensile properties of Ti-48Al-2Cr-2Nb alloy additively manufactured by electron beam melting, Additive Manufacturing 13 (2017) 61-70.

[43] P. Wang, M.L.S. Nai, S. Lu, J. Bai, B. Zhang, J. Wei, Study of direct fabrication of Ti-6Al-4V impeller on a wrought Ti-6Al-4V plate by electron beam melting, JOM (2017). https://doi.org/10.1007/s11837-017-2610-5.

[44] M. Seifi, A.A. Salem, D.P. Satko, U. Ackelid, S.L. Semiatin, J.J. Lewandowski, Effects of HIP on microstructural heterogeneity, defect distribution and mechanical properties of additively manufactured EBM Ti-48Al-2Cr-2Nb, Journal of Alloys and Compounds 729 (2017) 1118-1135.

[45] D. Deng, J. Moverare, R.L. Peng, H. Söderberg, Microstructure and anisotropic mechanical properties of EBM manufactured Inconel 718 and effects of post heat treatments, Materials Science and Engineering: A 693 (2017) 151-163.

[46] Y. Zhai, H. Galarraga, D.A. Lados, Microstructure, static properties, and fatigue crack growth mechanisms in Ti-6Al-4V fabricated by additive manufacturing: LENS and EBM, Engineering Failure Analysis 69 (2016) 3-14.

[47] Z. Sun, X. Tan, S.B. Tor, W.Y. Yeong, Selective laser melting of stainless steel 316L with low porosity and high build rates, Materials & Design 104 (2016) 197-204.

[48] X. Wang, K. Chou, Electron Backscatter Diffraction Analysis of Inconel 718 Parts Fabricated by Selective Laser Melting Additive Manufacturing, JOM 69(2) (2017) 402-408.

[49] X. Wang, K. Chou, Effects of thermal cycles on the microstructure evolution of Inconel 718 during selective laser melting process, Additive Manufacturing 18 (2017) 1-14.

[50] X. Wang, T. Keya, K. Chou, Build Height Effect on the Inconel 718 Parts Fabricated by Selective Laser Melting, Procedia Manufacturing 5 (2016) 1006-1017.

[51] K. Graff, M. Short, M. Norfolk, Very high power ultrasonic additive manufacturing (VHP UAM) for advanced materials, International Conference on Additive Manufacturing, 2010.

[52] M.R. Sriraman, S.S. Babu, M. Short, Bonding characteristics during very high power ultrasonic additive manufacturing of copper, Scripta Materialia 62(8) (2010) 560-563.

[53] T. Wang, Y.Y. Zhu, S.Q. Zhang, H.B. Tang, H.M. Wang, Grain morphology evolution behavior of titanium alloy components during laser melting deposition additive manufacturing, Journal of Alloys and Compounds 632 (2015) 505-513.

[54] J. Gockel, J. Beuth, K. Taminger, Integrated control of solidification microstructure and melt pool dimensions in electron beam wire feed additive manufacturing of Ti-6Al-4V, Additive Manufacturing 1–4 (2014) 119-126.

[55] K. Iwasaki, S. Ohkawa, M. Uo, T. Akasaka, F. Watari, Laser welding of titanium and dental precious alloys, Materials Transactions 45(4) (2004) 1140-1146.

[56] P. Heinl, L. Müller, C. Körner, R.F. Singer, F.A. Müller, Cellular Ti–6Al–4V structures with interconnected macro porosity for bone implants fabricated by selective electron beam melting, Acta Biomaterialia 4(5) (2008) 1536-1544.

[57] S. Biamino, A. Penna, U. Ackelid, S. Sabbadini, O. Tassa, P. Fino, M. Pavese, P. Gennaro, C. Badini, Electron beam melting of Ti–48Al–2Cr–2Nb alloy: Microstructure and mechanical properties investigation, Intermetallics 19(6) (2011) 776-781.

[58] B. Ferrar, L. Mullen, E. Jones, R. Stamp, C.J. Sutcliffe, Gas flow effects on selective laser melting (SLM) manufacturing performance, Journal of Materials Processing Technology 212(2) (2012) 355-364.

[59] W.J. Sames, K.A. Unocic, R.R. Dehoff, T. Lolla, S.S. Babu, Thermal effects on microstructural heterogeneity of Inconel 718 materials fabricated by electron beam melting, Journal of Materials Research 29(17) (2014) 1920-1930.

[60] X. Zhao, S. Li, M. Zhang, Y. Liu, T.B. Sercombe, S. Wang, Y. Hao, R. Yang, L.E. Murr, Comparison of the microstructures and mechanical properties of Ti–6Al–4V fabricated by selective laser melting and electron beam melting, Materials & Design 95 (2016) 21-31.

[61] X. Wang, K. Chou, Residual stress in metal parts produced by powder-bed additive manufacturing processes, proceedings of the 26th International solid freeform fabrication symposium, 2015, pp. 1463-1474.

[62] W.U.H. Syed, A.J. Pinkerton, L. Li, Combining wire and coaxial powder feeding in laser direct metal deposition for rapid prototyping, Applied Surface Science 252(13) (2006) 4803-4808.

[63] N.T. Aboulkhair, N.M. Everitt, I. Ashcroft, C. Tuck, Reducing porosity in AlSi10Mg parts processed by selective laser melting, Additive Manufacturing 1–4 (2014) 77-86.

[64] L. Thijs, F. Verhaeghe, T. Craeghs, J.V. Humbeeck, J.-P. Kruth, A study of the microstructural evolution during selective laser melting of Ti–6Al–4V, Acta Materialia 58(9) (2010) 3303-3312.

[65] L.N. Carter, C. Martin, P.J. Withers, M.M. Attallah, The influence of the laser scan strategy on grain structure and cracking behaviour in SLM powder-bed fabricated nickel superalloy, Journal of Alloys and Compounds 615 (2014) 338-347.

[66] M.F. Zaeh, M. Kahnert, The effect of scanning strategies on electron beam sintering, Production Engineering 3(3) (2009) 217-224.

[67] T. Ishimoto, K. Hagihara, K. Hisamoto, S.-H. Sun, T. Nakano, Crystallographic texture control of beta-type Ti–15Mo–5Zr–3Al alloy by selective laser melting for the development of novel implants with a biocompatible low Young's modulus, Scripta Materialia 132 (2017) 34-38.

[68] L. Thijs, K. Kempen, J.-P. Kruth, J. Van Humbeeck, Fine-structured aluminium products with controllable texture by selective laser melting of pre-alloyed AlSi10Mg powder, Acta Materialia 61(5) (2013) 1809-1819.

[69] L. Thijs, M.L. Montero Sistiaga, R. Wauthle, Q. Xie, J.-P. Kruth, J. Van Humbeeck, Strong morphological and crystallographic texture and resulting yield strength anisotropy in selective laser melted tantalum, Acta Materialia 61(12) (2013) 4657-4668.

[70] P. Kobryn, S. Semiatin, Mechanical properties of laser-deposited Ti-6Al-4V, Solid Freeform Fabrication Proceedings, Austin, 2001, pp. 6-8.

[71] H. Helmer, A. Bauereiß, R.F. Singer, C. Körner, Grain structure evolution in Inconel 718 during selective electron beam melting, Materials Science and Engineering: A 668 (2016) 180-187.

[72] R.R. Dehoff, M.M. Kirka, W.J. Sames, H. Bilheux, A.S. Tremsin, L.E. Lowe, S.S. Babu, Site specific control of crystallographic grain orientation through electron beam additive manufacturing, Materials Science and Technology 31(8) (2015) 931-938.

[73] A.B. Spierings, M. Voegtlin, T. Bauer, K. Wegener, Powder flowability characterisation methodology for powder-bed-based metal additive manufacturing, Progress in Additive Manufacturing 1(1) (2016) 9-20.

[74] N. Karapatis, G. Egger, P. Gygax, R. Glardon, Optimization of powder layer density in selective laser sintering, Proc. of Solid Freeform Fabrication Symposium 1999, 1999, pp. 255-263.

[75] A. Spierings, G. Levy, Comparison of density of stainless steel 316L parts produced with selective laser melting using different powder grades, Proceedings of the Annual International Solid Freeform Fabrication Symposium, Austin, TX, 2009, pp. 342-353.

[76] F. Wang, S. Williams, P. Colegrove, A.A. Antonysamy, Microstructure and Mechanical Properties of Wire and Arc Additive Manufactured Ti-6Al-4V, Metallurgical and Materials Transactions A 44(2) (2013) 968-977.

[77] S.H. Mok, G. Bi, J. Folkes, I. Pashby, J. Segal, Deposition of Ti–6Al–4V using a high power diode laser and wire, Part II: Investigation on the mechanical properties, Surface and Coatings Technology 202(19) (2008) 4613-4619.

[78] E. Brandl, B. Baufeld, C. Leyens, R. Gault, Additive manufactured Ti-6Al-4V using welding wire: comparison of laser and arc beam deposition and evaluation with respect to aerospace material specifications, Physics Procedia 5 (2010) 595-606.

[79] N. Hrabe, T. Quinn, Effects of processing on microstructure and mechanical properties of a titanium alloy (Ti–6Al–4V) fabricated using electron beam melting (EBM), Part 2: Energy input, orientation, and location, Materials Science and Engineering: A 573 (2013) 271-277.

[80] V. Cain, L. Thijs, J. Van Humbeeck, B. Van Hooreweder, R. Knutsen, Crack propagation and fracture toughness of Ti6Al4V alloy produced by selective laser melting, Additive Manufacturing 5 (2015) 68-76.

[81] P. Edwards, A. O'Conner, M. Ramulu, Electron beam additive manufacturing of titanium components: properties and performance, Journal of Manufacturing Science and Engineering 135(6) (2013) 061016.

[82] B. Baufeld, Effect of deposition parameters on mechanical properties of shaped metal deposition parts, Proceedings of the Institution of Mechanical Engineers, Part B: Journal of Engineering Manufacture 226(1) (2012) 126-136.

[83] N. Hrabe, T. Quinn, Effects of processing on microstructure and mechanical properties of a titanium alloy (Ti–6Al–4V) fabricated using electron beam melting (EBM), part 1: Distance from build plate and part size, Materials Science and Engineering: A 573 (2013) 264-270.

[84] X. Tan, Y. Kok, Y.J. Tan, M. Descoins, D. Mangelinck, S.B. Tor, K.F. Leong, C.K. Chua, Graded microstructure and mechanical properties of additive manufactured Ti–6Al–4V via electron beam melting, Acta Materialia 97 (2015) 1-16.

[85] S.S. Al-Bermani, M.L. Blackmore, W. Zhang, I. Todd, The Origin of Microstructural Diversity, Texture, and Mechanical Properties in Electron Beam Melted Ti-6Al-4V, Metallurgical and Materials Transactions A 41(13) (2010) 3422-3434.

[86] L. Qian, J. Mei, J. Liang, X. Wu, Influence of position and laser power on thermal history and microstructure of direct laser fabricated Ti–6Al–4V samples, Materials Science and Technology 21(5) (2005) 597-605.

[87] A. Takaichi, Suyalatu, T. Nakamoto, N. Joko, N. Nomura, Y. Tsutsumi, S. Migita, H. Doi, S. Kurosu, A. Chiba, N. Wakabayashi, Y. Igarashi, T. Hanawa, Microstructures and mechanical properties of Co–29Cr–6Mo alloy fabricated by selective laser melting process for dental applications, Journal of the Mechanical Behavior of Biomedical Materials 21 (2013) 67-76.

[88] L. Ladani, J. Razmi, S.F. Choudhury, Mechanical Anisotropy and Strain Rate Dependency Behavior of Ti6Al4V Produced Using E-Beam Additive Fabrication, Journal of Engineering Materials and Technology 136(3) (2014) 031006.

[89] J. Donoghue, A.A. Antonysamy, F. Martina, P.A. Colegrove, S.W. Williams, P.B. Prangnell, The effectiveness of combining rolling deformation with Wire–Arc Additive Manufacture on β-grain refinement and texture modification in Ti–6Al–4V, Materials Characterization 114 (2016) 103-114.

[90] A.A. Antonysamy, J. Meyer, P.B. Prangnell, Effect of build geometry on the β-grain structure and texture in additive manufacture of Ti6Al4V by selective electron beam melting, Materials Characterization 84 (2013) 153-168.

[91] L. Bian, S.M. Thompson, N. Shamsaei, Mechanical Properties and Microstructural Features of Direct Laser-Deposited Ti-6Al-4V, JOM 67(3) (2015) 629-638.

[92] S. Tammas-Williams, H. Zhao, F. Léonard, F. Derguti, I. Todd, P. Prangnell, XCT analysis of the influence of melt strategies on defect population in Ti–6Al–4V components manufactured by Selective Electron Beam Melting, Materials Characterization 102 (2015) 47-61.

[93] S.K. Everton, M. Hirsch, P. Stravroulakis, R.K. Leach, A.T. Clare, Review of in-situ process monitoring and in-situ metrology for metal additive manufacturing, Materials & Design 95 (2016) 431-445.

[94] ASTM, Standard Terminology for Additive Manufacturing-Coordinate Systems and Test Methodologies, ISO / ASTM52921-13, ASTM International, West Conshohocken, PA, 2013.

[95] F. Froes, B. Dutta, The Additive Manufacturing (AM) of Titanium Alloys, Advanced Materials Research, Trans Tech Publ, 2014, pp. 19-25.

[96] J. Alcisto, A. Enriquez, H. Garcia, S. Hinkson, T. Steelman, E. Silverman, P. Valdovino, H. Gigerenzer, J. Foyos, J. Ogren, J. Dorey, K. Karg, T. McDonald, O.S. Es-Said, Tensile Properties and Microstructures of Laser-Formed Ti-6Al-4V, Journal of Materials Engineering and Performance 20(2) (2011) 203-212.

[97] M. Simonelli, Y.Y. Tse, C. Tuck, Effect of the build orientation on the mechanical properties and fracture modes of SLM Ti–6Al–4V, Materials Science and Engineering: A 616 (2014) 1-11.

[98] C. Qiu, N.J.E. Adkins, M.M. Attallah, Microstructure and tensile properties of selectively laser-melted and of HIPed laser-melted Ti–6Al–4V, Materials Science and Engineering: A 578 (2013) 230-239.

[99] P. Wang, M.L.S. Nai, W.J. Sin, J. Wei, Effect of Building Height on Microstructure and Mechanical Properties of Big-Sized Ti-6Al-4V Plate Fabricated by Electron Beam Melting, MATEC Web of Conferences 30 (2015) 02001.

[100] S. Raghavan, M.L.S. Nai, P. Wang, W.J. Sin, T. Li, J. Wei, Heat Treatment of Electron Beam Melted (EBM) Ti-6Al-4V: Microstructure to Mechanical Property Correlations, Rapid Prototyping Journal (2017) doi: 10.1108/RPJ-05-2016-0070.

[101] T. Vilaro, C. Colin, J.D. Bartout, As-Fabricated and Heat-Treated Microstructures of the Ti-6Al-4V Alloy Processed by Selective Laser Melting, Metallurgical and Materials Transactions A 42(10) (2011) 3190-3199.

[102] M. Svensson, U. Ackelid, A. Ab, Titanium alloys manufactured with electron beam melting mechanical and chemical properties, Proceedings of Materials & Processes for Medical Devices Conference, 2010, pp. 189-194.

[103] H. Rafi, N. Karthik, H. Gong, T.L. Starr, B.E. Stucker, Microstructures and mechanical properties of Ti6Al4V parts fabricated by selective laser melting and electron beam melting, Journal of Materials Engineering and Performance 22(12) (2013) 3872-3883.

[104] A. Christensen, R. Kircher, A. Lippincott, Qualification of electron beam melted (EBM) Ti6Al4V-ELI for orthopaedic applications, Medical Device Materials IV: Proceedings of the Materials and Processes for Medical Devices Conference, 2008, pp. 48-53.

[105] R. Kircher, A. Christensen, K. Wurth, Electron Beam Melted (EBM) Co-Cr-Mo Alloy for Orthopaedic Implant Applications, Solid Freeform Fabrication Proceedings, 2009, pp. 428-36.

[106] J. Strößner, M. Terock, U. Glatzel, Mechanical and Microstructural Investigation of Nickel-Based Superalloy IN718 Manufactured by Selective Laser Melting (SLM), Advanced Engineering Materials 17(8) (2015) 1099-1105.

[107] I. Rosenthal, A. Stern, N. Frage, Microstructure and Mechanical Properties of AlSi10Mg Parts Produced by the Laser Beam Additive Manufacturing (AM) Technology, Metallography, Microstructure, and Analysis 3(6) (2014) 448-453.

[108] J. Suryawanshi, K.G. Prashanth, S. Scudino, J. Eckert, O. Prakash, U. Ramamurty, Simultaneous enhancements of strength and toughness in an Al-12Si alloy synthesized using selective laser melting, Acta Materialia 115 (2016) 285-294.

[109] N. Read, W. Wang, K. Essa, M.M. Attallah, Selective laser melting of AlSi10Mg alloy: Process optimisation and mechanical properties development, Materials & Design 65 (2015) 417-424.

[110] K. Kempen, L. Thijs, J. Van Humbeeck, J.-P. Kruth, Mechanical properties of AlSi10Mg produced by selective laser melting, Physics Procedia 39 (2012) 439-446.

[111] C. Song, Y. Yang, Y. Wang, D. Wang, J. Yu, Research on rapid manufacturing of CoCrMo alloy femoral component based on selective laser melting, The International Journal of Advanced Manufacturing Technology 75(1) (2014) 445-453.

[112] C. Qiu, G.A. Ravi, C. Dance, A. Ranson, S. Dilworth, M.M. Attallah, Fabrication of large Ti–6Al–4V structures by direct laser deposition, Journal of Alloys and Compounds 629 (2015) 351-361.

[113] Q. Zhang, J. Chen, Z. Zhao, H. Tan, X. Lin, W. Huang, Microstructure and anisotropic tensile behavior of laser additive manufactured TC21 titanium alloy, Materials Science and Engineering: A 673 (2016) 204-212.

[114] ASTM International, ASTM F1472-14, Standard Specification for Wrought Titanium-6Aluminum-4Vanadium Alloy for Surgical Implant Applications (UNS R56400), West Conshohocken, PA, 2014.

[115] ASTM International, ASTM F1108-14, Standard Specification for Titanium-6Aluminum-4Vanadium Alloy Castings for Surgical Implants (UNS R56406), West Conshohocken, PA, 2014.

[116] ASTM International, ASTM F75-12, Standard Specification for Cobalt-28 Chromium-6 Molybdenum Alloy Castings and Casting Alloy for Surgical Implants (UNS R30075), West Conshohocken, PA, 2012.

[117] ASTM International, ASTM F1537-11, Standard Specification for Wrought Cobalt-28Chromium-6Molybdenum Alloys for Surgical Implants (UNS R31537, UNS R31538, and UNS R31539), West Conshohocken, PA, 2011.

[118] J.G. Kaufman, Properties of aluminum alloys: tensile, creep, and fatigue data at high and low temperatures, ASM international1999.

[119] M.M. Kirka, F. Medina, R. Dehoff, A. Okello, Mechanical behavior of post-processed Inconel 718 manufactured through the electron beam melting process, Materials Science and Engineering: A 680 (2017) 338-346.

[120] L.A. Pruitt, Deformation, yielding, fracture and fatigue behavior of conventional and highly cross-linked ultra high molecular weight polyethylene, Biomaterials 26(8) (2005) 905-915.

[121] K.-H. Schwalbe, On the influence of microstructure on crack propagation mechanisms and fracture toughness of metallic materials, Engineering Fracture Mechanics 9(4) (1977) 795-832.

[122] P.O. Judt, A. Ricoeur, G. Linek, Crack Paths at Multiple-crack Systems in Anisotropic Structures: Simulation and Experiment, Procedia Materials Science 3 (2014) 2122-2127.

[123] G. Welsch, R. Boyer, E. Collings, Materials properties handbook: titanium alloys, ASM international1993.

[124] D. Cameron, D. Hoeppner, Fatigue properties in engineering, ASM International, ASM Handbook. 19 (1996) 15-26.

[125] P. Edwards, M. Ramulu, Effect of build direction on the fracture toughness and fatigue crack growth in selective laser melted Ti-6Al-4 V, Fatigue & Fracture of Engineering Materials & Structures 38(10) (2015) 1228-1236.

[126] X. Gong, T. Anderson, K. Chou, Review on powder-based electron beam additive manufacturing technology, Manufacturing Review 1 (2014) 2.

[127] N. Ikeo, T. Ishimoto, A. Serizawa, T. Nakano, Control of mechanical properties of three-dimensional Ti-6Al-4V products fabricated by electron beam melting with unidirectional

elongated pores, Metallurgical and Materials Transactions A: Physical Metallurgy and Materials Science 45(10) (2014) 4293-4301.

[128] R. Wauthle, B. Vrancken, B. Beynaerts, K. Jorissen, J. Schrooten, J.-P. Kruth, J. Van Humbeeck, Effects of build orientation and heat treatment on the microstructure and mechanical properties of selective laser melted Ti6Al4V lattice structures, Additive Manufacturing 5 (2015) 77-84.

[129] O. Cansizoglu, O. Harrysson, D. Cormier, H. West, T. Mahale, Properties of Ti–6Al–4V non-stochastic lattice structures fabricated via electron beam melting, Materials Science and Engineering: A 492(1–2) (2008) 468-474.

[130] P. Li, D.H. Warner, A. Fatemi, N. Phan, Critical assessment of the fatigue performance of additively manufactured Ti–6Al–4V and perspective for future research, International Journal of Fatigue 85 (2016) 130-143.

[131] B.L. Boyce, R.O. Ritchie, Effect of load ratio and maximum stress intensity on the fatigue threshold in Ti–6Al–4V, Engineering Fracture Mechanics 68(2) (2001) 129-147.

[132] J. Ding, R. Hall, J. Byrne, Effects of stress ratio and temperature on fatigue crack growth in a Ti–6Al–4V alloy, International Journal of Fatigue 27(10–12) (2005) 1551-1558.

[133] R. Hague, S. Mansour, N. Saleh, Material and design considerations for rapid manufacturing, International Journal of Production Research 42(22) (2004) 4691-4708.

[134] X. Tan, Y. Kok, Y.J. Tan, G. Vastola, Q.X. Pei, G. Zhang, Y.-W. Zhang, S.B. Tor, K.F. Leong, C.K. Chua, An experimental and simulation study on build thickness dependent microstructure for electron beam melted Ti–6Al–4V, Journal of Alloys and Compounds 646 (2015) 303-309.

[135] M. Seifi, A. Salem, J. Beuth, O. Harrysson, J.J. Lewandowski, Overview of Materials Qualification Needs for Metal Additive Manufacturing, JOM 68(3) (2016) 747-764.

[136] X. Tan, Y. Kok, W.Q. Toh, Y.J. Tan, M. Descoins, D. Mangelinck, S.B. Tor, K.F. Leong, C.K. Chua, Revealing martensitic transformation and α/β interface evolution in electron beam melting three-dimensional-printed Ti-6Al-4V, Scientific reports 6 (2016).

[137] P. Wang, M.L.S. Nai, X. Tan, G. Vastola, R. Srinivasan, W.J. Sin, S.B. Tor, Q.X. Pei, J. Wei, Recent Progress of Additive Manufactured Ti-6Al-4V by Electron Beam Melting, 2016 Annual International Solid Freeform Fabrication Symposium (SFF Symp 2016), Austin, Texas, USA, 2016, pp. 691-704.

[138] W. Xu, M. Brandt, S. Sun, J. Elambasseril, Q. Liu, K. Latham, K. Xia, M. Qian, Additive manufacturing of strong and ductile Ti–6Al–4V by selective laser melting via in situ martensite decomposition, Acta Materialia 85 (2015) 74-84.

[139] S.-H. Sun, Y. Koizumi, S. Kurosu, Y.-P. Li, H. Matsumoto, A. Chiba, Build direction dependence of microstructure and high-temperature tensile property of Co–Cr–Mo alloy fabricated by electron beam melting, Acta Materialia 64 (2014) 154-168.

[140] S.-H. Sun, Y. Koizumi, S. Kurosu, Y.-P. Li, A. Chiba, Phase and grain size inhomogeneity and their influences on creep behavior of Co–Cr–Mo alloy additive manufactured by electron beam melting, Acta Materialia 86 (2015) 305-318.

[141] Y.H. Kok, X.P. Tan, N.H. Loh, S.B. Tor, C.K. Chua, Geometry dependence of microstructure and microhardness for selective electron beam-melted Ti–6Al–4V parts, Virtual and Physical Prototyping 11(3) (2016) 183-191.

[142] S.M. Kelly, S.L. Kampe, Microstructural evolution in laser-deposited multilayer Ti-6Al-4V builds: Part I. Microstructural characterization, Metallurgical and Materials Transactions A 35(6) (2004) 1861-1867.

[143] F. Martina, P.A. Colegrove, S.W. Williams, J. Meyer, Microstructure of Interpass Rolled Wire + Arc Additive Manufacturing Ti-6Al-4V Components, Metallurgical and Materials Transactions A 46(12) (2015) 6103-6118.

[144] J.Y. Guédou, C. Körner, H. Helmer, A. Bauereiß, R.F. Singer, J. Choné, Tailoring the grain structure of IN718 during selective electron beam melting, MATEC Web of Conferences 14 (2014) 08001.

[145] K. Hagihara, T. Nakano, M. Suzuki, T. Ishimoto, Suyalatu, S.-H. Sun, Successful additive manufacturing of MoSi2 including crystallographic texture and shape control, Journal of Alloys and Compounds 696 (2017) 67-72.

[146] L.E. Murr, E.V. Esquivel, S.A. Quinones, S.M. Gaytan, M.I. Lopez, E.Y. Martinez, F. Medina, D.H. Hernandez, E. Martinez, J.L. Martinez, S.W. Stafford, D.K. Brown, T. Hoppe, W. Meyers, U. Lindhe, R.B. Wicker, Microstructures and mechanical properties of electron beam-rapid manufactured Ti–6Al–4V biomedical prototypes compared to wrought Ti–6Al–4V, Materials Characterization 60(2) (2009) 96-105.

[147] A.R. Nassar, J.S. Keist, E.W. Reutzel, T.J. Spurgeon, Intra-layer closed-loop control of build plan during directed energy additive manufacturing of Ti–6Al–4V, Additive Manufacturing 6 (2015) 39-52.

[148] T. Machry, D. Eatock, J. Meyer, A. Antonysamy, A. Ho, P. Prangnell, Effect of microstructure on the tensile strength of Ti6Al4V specimens manufactured using additive manufacturing electron beam process, Powder Metallurgy 59(1) (2016) 41-50.

[149] T. Amine, J.W. Newkirk, F. Liou, Methodology for Studying Effect of Cooling Rate During Laser Deposition on Microstructure, Journal of Materials Engineering and Performance 24(8) (2015) 3129-3136.

[150] N. Yu, Process parameter optimization for direct metal laser sintering (DMLS), Department of Mechanical Engineering, National University of Singapore, Singapore, 2005.

[151] W. Toh, P. Wang, X. Tan, M. Nai, E. Liu, S. Tor, Microstructure and Wear Properties of Electron Beam Melted Ti-6Al-4V Parts: A Comparison Study against As-Cast Form, Metals 6(11) (2016) 284.

[152] M. Jamshidinia, M.M. Atabaki, M. Zahiri, S. Kelly, A. Sadek, R. Kovacevic, Microstructural modification of Ti–6Al–4V by using an in-situ printed heat sink in Electron Beam Melting® (EBM), Journal of Materials Processing Technology 226 (2015) 264-271.

[153] P.W. Chaoyi He, Mui Ling Sharon Nai, Jun Wei, Distribution of porosity in electron beam melting additive manufactured Ti-6Al-4V component, The Ninth Pacific Rim International Conference on Advanced Materials and Processing (PRICM9), The Japan Institute of Metals and Materials, 2016, pp. 385-387.

[154] R. Cunningham, S.P. Narra, T. Ozturk, J. Beuth, A.D. Rollett, Evaluating the Effect of Processing Parameters on Porosity in Electron Beam Melted Ti-6Al-4V via Synchrotron X-ray Microtomography, JOM 68(3) (2016) 765-771.

[155] B. Song, S. Dong, Q. Liu, H. Liao, C. Coddet, Vacuum heat treatment of iron parts produced by selective laser melting: Microstructure, residual stress and tensile behavior, Materials & Design 54 (2014) 727-733.

[156] K.N. Amato, S.M. Gaytan, L.E. Murr, E. Martinez, P.W. Shindo, J. Hernandez, S. Collins, F. Medina, Microstructures and mechanical behavior of Inconel 718 fabricated by selective laser melting, Acta Materialia 60(5) (2012) 2229-2239.

[157] E. Brandl, D. Greitemeier, Microstructure of additive layer manufactured Ti–6Al–4V after exceptional post heat treatments, Materials Letters 81 (2012) 84-87.

[158] S.L. Lu, H.P. Tang, Y.P. Ning, N. Liu, D.H. StJohn, M. Qian, Microstructure and Mechanical Properties of Long Ti-6Al-4V Rods Additively Manufactured by Selective Electron Beam Melting Out of a Deep Powder Bed and the Effect of Subsequent Hot Isostatic Pressing, Metallurgical and Materials Transactions A (2015) 1-11.

[159] H. Galarraga, D.A. Lados, R.R. Dehoff, M.M. Kirka, P. Nandwana, Effects of the microstructure and porosity on properties of Ti-6Al-4V ELI alloy fabricated by electron beam melting (EBM), Additive Manufacturing 10 (2016) 47-57.

[160] Y.Y. Sun, S. Gulizia, D. Fraser, C.H. Oh, S.L. Lu, M. Qian, Layer Additive Production or Manufacturing of Thick Sections of Ti-6Al-4V by Selective Electron Beam Melting (SEBM), JOM 69(10) (2017) 1836-1843.

[161] S. Palanivel, A.K. Dutt, E.J. Faierson, R.S. Mishra, Spatially dependent properties in a laser additive manufactured Ti–6Al–4V component, Materials Science and Engineering: A 654 (2016) 39-52.

[162] S. Das, M. Wohlert, J.J. Beaman, D.L. Bourell, Processing of titanium net shapes by SLS/HIP, Materials & Design 20(2–3) (1999) 115-121.

[163] D.A. Ramirez, L.E. Murr, E. Martinez, D.H. Hernandez, J.L. Martinez, B.I. Machado, F. Medina, P. Frigola, R.B. Wicker, Novel precipitate–microstructural architecture developed in the fabrication of solid copper components by additive manufacturing using electron beam melting, Acta Materialia 59(10) (2011) 4088-4099.

[164] H. Shiratori, T. Fujieda, K. Yamanaka, Y. Koizumi, K. Kuwabara, T. Kato, A. Chiba, Relationship between the microstructure and mechanical properties of an equiatomic AlCoCrFeNi high-entropy alloy fabricated by selective electron beam melting, Materials Science and Engineering: A 656 (2016) 39-46.

[165] A. Hinojos, J. Mireles, A. Reichardt, P. Frigola, P. Hosemann, L.E. Murr, R.B. Wicker, Joining of Inconel 718 and 316 Stainless Steel using electron beam melting additive manufacturing technology, Materials & Design 94 (2016) 17-27.

[166] S. Sun, L. Zheng, H. Peng, H. Zhang, Microstructure and mechanical properties of Al-Fe-V-Si aluminum alloy produced by electron beam melting, Materials Science and Engineering: A 659 (2016) 207-214.

[167] G. Kasperovich, J. Hausmann, Improvement of fatigue resistance and ductility of TiAl6V4 processed by selective laser melting, Journal of Materials Processing Technology 220 (2015) 202-214.

[168] Z. Wang, K. Guan, M. Gao, X. Li, X. Chen, X. Zeng, The microstructure and mechanical properties of deposited-IN718 by selective laser melting, Journal of Alloys and Compounds 513 (2012) 518-523.

[169] L. Zheng, Y. Liu, S. Sun, H. Zhang, Selective laser melting of Al–8.5Fe–1.3V–1.7Si alloy: Investigation on the resultant microstructure and hardness, Chinese Journal of Aeronautics 28(2) (2015) 564-569.

[170] L. Costa, R. Vilar, T. Reti, A.M. Deus, Rapid tooling by laser powder deposition: Process simulation using finite element analysis, Acta Materialia 53(14) (2005) 3987-3999.

[171] G. Vastola, G. Zhang, Q. Pei, Y.-W. Zhang, Modeling the Microstructure Evolution During Additive Manufacturing of Ti6Al4V: A Comparison Between Electron Beam Melting and Selective Laser Melting, JOM 68(5) (2016) 1370-1375.

[172] J. Irwin, E.W. Reutzel, P. Michaleris, J. Keist, A.R. Nassar, Predicting Microstructure From Thermal History During Additive Manufacturing for Ti-6Al-4V, Journal of Manufacturing Science and Engineering 138(11) (2016) 111007-111007.

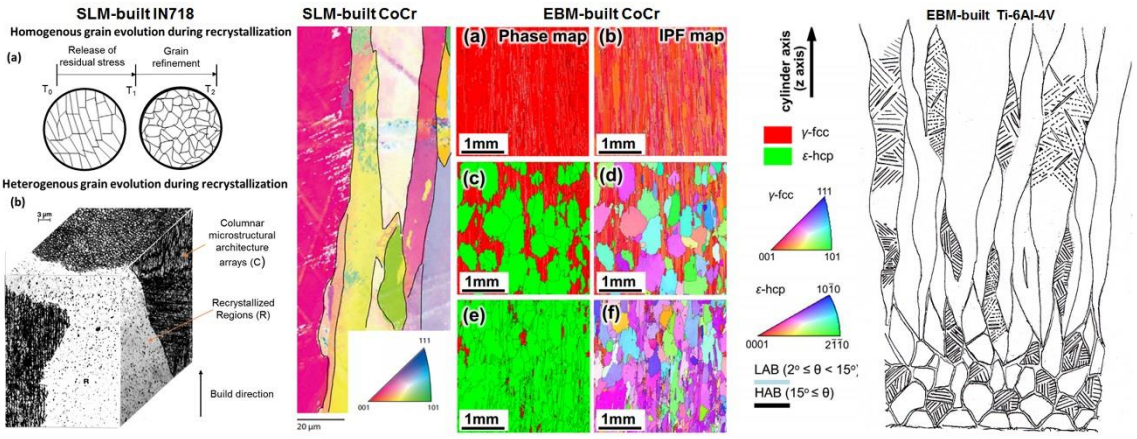

Graphical abstract

Highlights

- The major metal AM systems and their processing conditions
- Contributing factors on anisotropy and heterogeneity of microstructure and mechanical properties in metal AM parts
- A critical review on anisotropic and heterogeneous mechanical properties of various metal AM parts
- State-of-the-art development in numerical modelling to predict anisotropy and heterogeneity in metal AM parts